

Alma Mater Studiorum – Università di Bologna

SCUOLA DI INGEGNERIA E ARCHITETTURE
DIPARTIMENTO DI INGEGNERIA INDUSTRIALE
Campus di Cesena

Laurea
in
INGEGNERIA BIOMEDICA

*Influence of Metastases' Location and Size on the Strain
Field Distribution in Metastatically Involved Human
Vertebrae:
An In Vitro Study*

Tesi in
COMPORTAMENTO MECCANICO DEI MATERIALI E BIOMATERIALI, C.I.

PRESENTATO DA:
Michele Serra

RELATORE:
Chiar.mo Prof. Luca Cristofolini

CORRELATORE:
Dott. Ing. Marco Palanca

Table of Contents

Abstract (EN)	1
Abstract (IT)	2
Nomenclature	3
Introduction	4
A Structural Overview of the Spine.....	7
The Metastasis	8
Studying the Mechanics of Metastatic Vertebrae	10
<i>In Vitro</i> Studies.....	10
<i>In Silico</i> Studies.....	11
The Mechanics of Metastatic Vertebrae in the Literature	13
Available Literature.....	13
The Aim of this Study.....	16
Materials & Methods	17
Specimens	17
Acquisition and Storage	17
Clinical CT and Consultation.....	18
Preparation and Alignment.....	18
Digital Image Correlation (DIC).....	23
A General Overview.....	23
Considerations on the Set-up.....	25
The Digital Noise	26
The Set-up for this Study	26
Test.....	29

Test: Surface Preparation	29
Set-up Adjustment.....	30
Test Design.....	31
Mechanical Testing	32
Assessment of the Position and Size of the Metastases	33
The Mask.....	33
Tests for the Intra-Operator Repeatability	35
Tests for the Inter-Operator Repeatability	36
Assessing Lytic Metastases Size	36
Application of Mask and Model.....	36
Metric	38
Results	39
Quantitative and Qualitative Analysis	39
Specimen 773	40
Specimen 775	42
Specimen 779	46
Specimen 784	50
Specimen 785	52
Metastases Size	55
Repeatability Tests.....	56
Results of Test for Intra-Operator Repeatability	56
Results of Test for Inter-Operator Repeatability	56
Discussion	58
Conclusions	62
Addendum	63
Additional Information from the CT-generated DICOM Files.....	63

Loading Criteria	64
Designing the Process of Mask Creation	66
Details Regarding Inter-/Intra- Operator Tests	68
References.....	78

Abstract (EN)

As the survival time for the patient affected by metastatic cancer increases, the current clinical practice is shifting towards therapies that aim at increasing their quality of life.

In order to that, the mechanics of metastatic tissue must be explored.

With this study, we decided to focus on the investigation of the mechanical behavior of metastatically involved vertebrae.

We focused our attention on size and location of lesions within the vertebral body; a debated topic, for whom no definitive study is available.

Eight segments of various length were obtained from five spines, involved with different type of metastatic lesions (i.e. osteolytic and osteoblastic).

The segments were tested with a combination of compression and anterior bending, their field of strains distribution was captured via DIC.

The field of strains distribution was analyzed both quantitatively and qualitatively.

Anteriorly located lesions were found to strongly influence the field of strains distribution, regardless of the size. The influence of posteriorly located lesions was found to be negligible.

The field of strain for vertebrae with mixed and blastic metastases was homogeneous, with strains of low magnitude, even under significant loads (i.e. 1.5BW).

Furthermore, a “tool” was designed to locate the lesions within the vertebral body starting from the CT scans. This “tool” was composed by a custom-design mask and a simple geometrical model for the study the lesions’ size.

We concluded that the field of strain distribution is primarily influenced by the metastasis type.

In case of lytic only metastasis, the location’s influence over strains is more significant that the influence of the size.

Abstract (IT)

Con l'aumento della speranza di vita per pazienti afflitti da metastasi, l'attuale pratica clinica tende ad orientarsi verso terapie che ne possano aumentare la qualità della vita.

Per fare ciò è necessario esplorare la meccanica del tessuto metastatico.

Con questo lavoro abbiamo deciso di concentrarci sullo studio del comportamento meccanico di vertebre metastatiche.

Abbiamo rivolto la nostra attenzione alla posizione e alla dimensione della lesione all'interno del corpo vertebrale; un argomento di dibattito per il quale non è disponibile nessuno studio conclusivo.

Otto segmenti di varia lunghezza sono stati ottenuti da cinque colonne vertebrali, con metastasi di differente tipo (i.e. osteolitico e osteoblastico).

I segmenti sono stati testati con una combinazione compressione e flessione anteriore, la distribuzione del campo di deformazione registrata per mezzo di DIC.

La distribuzione del campo di deformazione è stata analizzata sia quantitativamente che qualitativamente.

Le lesioni localizzate anteriormente risultavano influenzare fortemente la distribuzione del campo di deformazione, a prescindere dalla loro dimensione. L'influenza di lesioni posizionate posteriormente era trascurabile.

Le vertebre con metastasi litiche e blastiche mostravano campi omogenei con deformazioni di bassa intensità, anche se sottoposte a carichi significativi (i.e. 1.5 BW).

In aggiunta, è stato progettato uno "strumento" per la localizzazione delle lesioni nel corpo vertebrale a partire dagli scan CT. Questo "strumento" era composto di maschere personalizzabili e di un semplice modello geometrico per studiare la dimensione delle lesioni,

Abbiamo concluso che la distribuzione del campo di deformazione è principalmente influenzata dal tipo di metastasis.

Nel caso di metastasi litiche, l'influenza della posizione sulle deformazioni è più significativa di quella della dimensione.

Nomenclature

In the following work we will often use this nomenclature:

BW = body weight

CC = cranio-caudal

CT = computed tomography

CAD = computed-aided design

DIC = Digital Image Correlation

DVC = Digital Volume Correlation

DOF = degrees of freedom

eps = engineering principal strains

eps1 = maximum engineering principal strains

eps2 = minimum engineering principal strains

FEA = finite element analysis

FEM = finite element model

FOV = field of view

MSV = mean strain value

NMSV = normalized mean strain value

QCT/FEA = quantitative computed tomography-based finite element analysis

QCT/FEM = quantitative computed tomography-based finite element model

PMMA = Polymethylmethacrylate

RL = right-left

ROI = region of interest

SD = standard deviation

SINS = Spine Instability Neoplastic Score

SMS = spinal motion segment

VB = vertebral body

Chapter 1: Introduction

Cancer is one of the most compelling topics for medical research, now more than ever. During the last decades, cancer registered a growth in incidence and mortality (figure 1). While pointing out the causes of this growth results to be an arduous task, one can argue that the aging, the growth of the population, and the changes due to socioeconomic development might be some of the driving factors (Bray, et al., 2018, p. 395).

In 2015, World Health Organization (WHO) estimated that cancer was the first cause of premature death in 46 countries out of 172.

Lung, breast and prostate cancers are the most common forms of cancer. Lung cancer involves 11.6% of the diagnosis and it is the main cause of cancer-related deaths (18.4%). Breast and prostate cancer follow closely (Bray, et al., 2018, p. 394-395).

Lung, breast and prostate cancers share the common tendency of forming bone metastases once in advanced phases. The risk of forming these metastases increases as the patient continues to live with the disease. At the time of death, chances are high that the bulk of the tumor will be localized in the bone (Mundy, 2002, p. 584).

While it is true that cure is no longer possible once cancer has metastasized in the skeleton, metastatic cancer is becoming a condition with which the patient must live for a significant amount of time.

As of today, 2-4 years is the median survival time for patient with metastatic breast cancer (Chung & Carlson, 2003). A significant lapse of time in comparison to the 24 months reported in the last century (Coleman & Rubens, 1987, p. 63).

Current clinical practice focuses on increasing the patient's quality of life during this period.

Of all the bone-affecting neoplasms, spinal metastases constitute a serious threat to the patient quality of life.

In addition to severe pain and hypercalcemia (typical consequences of bone metastases), spinal neoplasms expose the patient to the risk of neurological damage and pathological fractures (even when performing trifle tasks).

To prevent the occurrence of these events, prophylactic measures could be adopted. An example of such measures is the prophylactic repair of bone tissue (Griesmann & Schüttemeyer, 1947).

However, such intervention should be pondered carefully as they expose the patient to nigh-unbearable invasive treatment. The combination of long operating time, blood loss, and postoperative complications might take its toll on the weakened body.

As such, studies should be performed to assess the mechanical parameters underlying the risk of bone failure. This would elicit a virtuous cycle that could, in the end, lead to a more careful use of the prophylactic therapies.

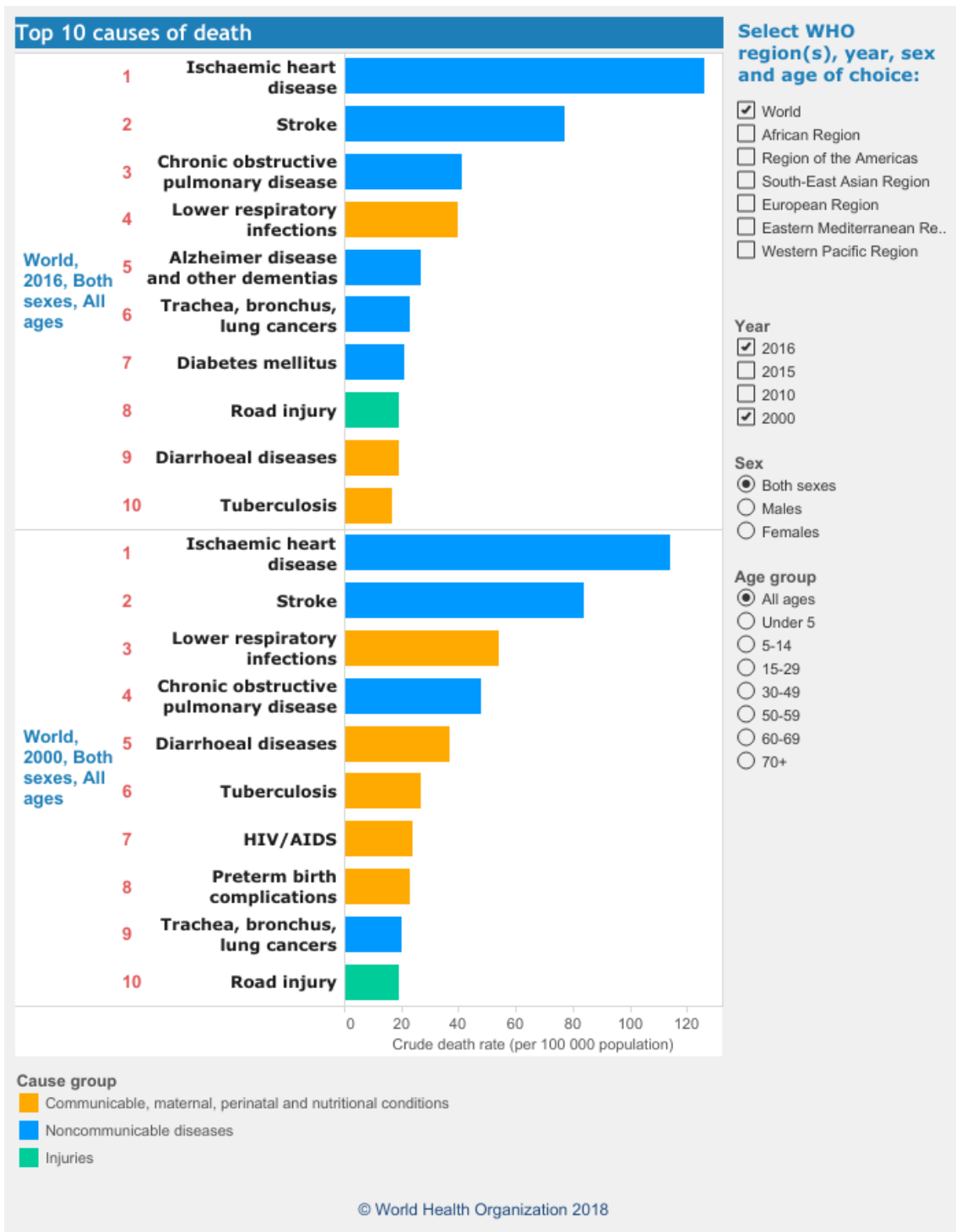


Figure 1 - Comparison of the top 10 causes of death (worldwide) in the years 2016 and 2000. While stroke and ischemic heart disease remain on the two top positions, trachea, bronchus, and lung cancers have registered a significant growth, passing from being the ninth to be the sixth causes of death.

1.1 A Structural Overview of the Spine

The vertebral column, or spine, holds an essential role in the human skeleton. It sustains the trunk. It provides an anchorage for muscles and ribs. It shells the spinal cord and the nerves from mechanical damages. It is involved in hemopoiesis.

The spine is in general constituted by 33 vertebrae. Each couple of vertebrae (except for the presacral and the first two cervical segments) is divided by a fibrocartilaginous disc (the intervertebral disc).

The spine can be divided in five sections: cervical, thoracic, lumbar, sacral and coccyx. The morphology of the spine is highly optimized, both internally and externally. The same goes for the single vertebrae. The morphology is influenced externally by mechanical and environmental factors, and internally by genetic, metabolic, and hormonal factors.

This results in a complex structure, capable of withstand the wide variety of loading scenarios pertaining both the physiological and non-physiological spheres.

Compression, torsion, bending and shear are commonly generated by everyday activities. Compression remains the predominant form of stress to whom the vertebra is subject. This predominance is reflected by the non-random distribution of the trabeculae in the cancellous bone of vertebral body. These are aligned with the axial forces acting on the vertebrae, which engender most of the strains on the vertebral body (Cristofolini, 2015, p. 792), in accordance with the so-called “Wolff’s law” (Wolff, 1892).

The complex structure of the spine and its subunits poses very specific problem to mechanical studies.

For instance, it is difficult to define the behavior of single vertebrae amidst the spine. In a functional spinal unit (FSU), each vertebra shows, although with limited extent, all 6 DOF (degrees of freedom).

In addition, most of the mechanical analysis performed on the long bones cannot be extended to the vertebrae. Vertebrae are irregular bones, thus beam’s theory results to be unsuitable for their study (unlike long bones, for which the Saint-Venant’s principle is often applied).

1.2 The Metastasis

A cancer is a tumor whose cells undergo uncontrolled mitosis, producing a tissue with different features from original. It tends to invade nearby organs and can propagate to the entire body through blood and lymphatic circulation.

A metastasis is the byproduct of a cancer. Their development is due to the diffusion of malignant cells detached from a primary tumor (Anonymous, 2019).

Each type of cancer has preferential sites to metastasize, and each metastasis can elicit different reactions. Subsequently, metastases' distribution tends to follow a specific trend, at times dependent on the primary tumor.

Hypothesis have been made about the causes of the non-random distribution of metastases within the body.

The first hypothesis dates to 1889, when Stephen Paget published on Lancet an article with his remark on the tendency of breast cancer to form metastases on bones (Paget, 1889). Paget's hypothesis identifies a "seed and soil" relation between the metastases and the bones: "When a plant goes to seed, its seeds are carried in all directions; but they can only live and grow if they fall on congenial soil" (Paget, 1889, p. 571). Being rich in growth factors, the bone results to be the "congenial soil" for the growth of metastases, hence the reason of the trend.

In 1928, James Ewing proposed a hypothesis on metastases' spread based on the blood flow and the lymphatic system (Ewing, 1922), thus explaining the formation of metastases in the liver and the lymph nodes.

In 1940, Oscar Batson, studying metastases in prostate cancer, proposed a new hypothesis with the veins at its core. According to Batson, the flow in veins can be reversed and "During these reversals a pathway up and down the spine exists which does not involve the heart or the lungs" (Batson, 1940, p. 145). Consequently, it is explained the presence of metastases in the spine and their absence in lungs and heart. Batson's hypothesis might effectively shed light upon prostate cancer metastasization in the spine (Mundy, 1997, p. 1547).

In 2002, Isaiah Fidler proposed a new outlook on Paget's "seed and soil" hypothesis. Fidler identified three principle, lying at the foundation of Paget's hypothesis. First,

neoplasms are heterogeneous; they contain subpopulations of cells with different angiogenic, invasive, and metastatic properties. Second, the process of metastasis is selective, only cells that survive in attaining the organ can metastasize. Third, the process depends on multiple interactions between metastatic cells and homeostatic factors (which can promote growth and survival of the cells, for instance) (Fidler, 2002, p. 499).

Being rich in growth factor and highly vascularized, the bones are a prime spot for the formation of metastasis, according to both Paget and Batson 's hypothesis.

Spine is a most weak spot. It is rich in blood vessels and growth factor, as well as near to the origin of the most common cancers (i.e. prostate, breast and lungs). Thus, the vertebrae are susceptible to the formation of metastases.

Bone metastases can form two types of lesions: osteolytic and osteoblastic.

Osteolytic lesions are destructive, as they are marked by an increased activity of osteoclasts. They are commonly associated with breast cancer.

Osteoblastic lesions are associated with an increased activity of osteoblasts. They are predominant in prostate cancer (Mundy, 1997, p. 1546-1547).

Osteolytic lesions do not prevent the formation osteoblastic ones, and *vice versa*. The classification of metastasis as lytic and blastic is but the representation of "two extremes of a continuum" in which falls each and every case (Roodman, 2004, p. 1655).

The development of bone metastases is often associated with various clinical consequences.

Lesions, be they osteoblastic or osteolytic, can cause severe bone pain.

Metastatic vertebra is also prone to undergo pathologic fractures, when lytic lesions are involved. These fracture (i.e. burst fractures) are often impending and can occur even in scenarios involving trivial loads.

A typical clinical consequence of vertebral fractures is neural damage. The fracture of the vertebral body can lead to the compression of the spina cord.

In osteoblastic lesions, nerve compression can also occur when new bony tissue grows obtruding onto nerves.

Hypercalcemia is a frequent consequence of lytic lesions. Bone resorption, due to the increased activity of osteoclasts, causes the raise of calcium levels, beyond the physiological ranges (Mundy, 1997, p. 1548).

1.3 Studying the Mechanics of Metastatic Vertebrae

In the next pages, we will mention various studies regarding the mechanics of the metastatic backbone. Hence, we will make a brief introduction about the methodologies to which research groups resort most frequently.

We will focus on the “instability” of the spine.

As of today, what “instability” is remains a topic of discussion. The definitions available are generally tailored and context specific.

Metastatically involved vertebrae show a propensity to undergo fracture when loadings within the physiological range are involved (Tschirhart, Nagpurkar, & Whyne, 2004, p. 653). Hence, we will define as “instable” a vertebra that might show this tendency.

Our interest (as that of other studies) is oriented toward the factors leading to fracture in a metastatically involved vertebra and the mechanisms of fracture. Knowing how a fracture takes place can prove useful to ascertain whether a certain vertebra is at risk and if prophylactic stabilization should be performed.

Some of the referenced studies will focus on the mechanical and structural properties (i.e. stiffness, failure strength, and mode of failure of a vertebral body or a disc).

Our study will focus on the comparison between healthy and pathological condition.

These studies can be conducted either *in vitro* or *in silico*.

1.3.1 Studying the Mechanics of Metastatic Vertebrae: *In Vitro* Studies

In Vitro study can be performed on human or animal vertebrae. The vertebrae can have actual or simulated defects¹.

An animal model, in certain cases, could be preferred to the use of human specimen. Firstly, because human specimens are difficult to obtain (being subject to a strict ethical regulation). Secondly, because there is lesser variability among specimens from farm-bred animals. However, animal models generally have a reduced validity, since they differ

¹ Note that simulated defects can only be osteolytic. To study an osteoblastic defect, a vertebra with actual defects must be tested. The reason resides in the fact that the new bony tissue (whose generation is due to the metastases) has properties that might differ from those of a healthy one.

anatomically from human specimen and their internal structure reflects a significantly different loading scenario (i.e. biped *versus* quadruped).

Human models are difficult to realize. Obtaining human specimen is difficult and the specimens generally feature a great variability (due to gender, age, pathology, ethnicity and so on). The benefits deriving from the use of a human model are well known.

As mentioned above, the investigation of spinal metastases might use either vertebrae with actual or simulated defects.

The simulation of lytic defects is a common practice. Defects are produced on the vertebral body by mean of needles, drills, *et cetera*.

While in theory far more adequate, the use of specimen with actual metastatic defects can be problematic. These specimens are harder to obtain and their lesions highly variable.

The preparation of the specimens (human or animal) might be needed. This phase might involve the removal of muscles, ligaments, tendons, and other soft tissues, the alignment, etc.

After being prepared, the specimens are tested. Test can be performed by applying either a set of known motions or a set of moments and forces. The test, in general, can aim to replicate ordinary motor tasks through the application of simplified loading (for a better control).

Preconditioning is generally performed prior to test, and allows the testing setup to settle, and to reduce the viscoelasticity (Brandolini, Cristofolini, & Viceconti, 2013, p. 1430002(16)).

1.3.2 Studying the Mechanics of Metastatic Vertebrae: *In Silico* Studies

While an *in silico* analysis will not be employed in this study, a brief introduction is needed.

In fact, in the literature, the mechanical behavior of a metastatically involved vertebra is often investigated through numerical models. Notably, finite element models (FEMs) and quantitative computed tomography-based finite element models (QCT/FEMs) are commonly employed in various studies.

In FEM, a real structure is discretized. The discrete model is composed by elements, defined by a series of interconnected points, or *nodes*. While the real structure is associated with a continuum problem with infinite degrees of freedom, the discretized

model has a limited number of DOF and thus can be solved computationally (Ratner, Hoffman, Schoen, & Lemons, 2013, p. 22).

A QCT/FEM is a FEM based on a QCT scans². It allows to create highly patient-specific FEM of bone segments from CT scans (Brandolini, Cristofolini, & Viceconti, 2013, p. 1430002(20)).

The use of numerical models has certain advantages over *in vitro* test. Firstly, additional measurements can be feasibly acquired, while *in vitro* tests are constrained by the need of further instrumenting the specimen (rising the costs and the complexity of the experiment). Secondly, a numerical model allows the repetition of tests (e.g. destructive test) that can be performed only once *in vitro*. Lastly, the boundary conditions and the test configuration can be changed without a significant increase of cost and labor.

On the other hand, numerical models remain a representation of reality, not reality itself, and, moreover, a discretization of a continuum problem.

In the case of the study of metastases, an *in silico* study would require a certain knowledge of the metastatic tissue. Although we can find several *in silico* studies in the literature, we still lack the knowledge necessary for an accurate modelization of the metastasis. In general, the available studies use the model that can better replicate the behavior of a metastatic tissue in a predetermined condition; however, there are no guaranties for the model to represent the reality outside the set of known parameters.

Ultimately, the reliability of a numerical model can be achieved only through a diligent validation, which relies on a series of *in vitro* testing.

² Quantitative Computed Tomography is a test to measure BMD (Bone Mineral Density). It is performed by mean of CT scanners. (Anonymous, 2019)

1.4 The Mechanics of Metastatic Vertebrae in the Literature

The literature about metastatically involved vertebra generally focuses on its mechanical competence and structural properties. The aim of the studies can be various: achieving a better understanding of metastatic lesions, validating *in silico* models, studying the effect of a therapy, finding parameters to assess the “stability”.

1.4.1 The Mechanics of Metastatic Vertebrae in the Literature: Available Literature

In preparation for the study, we had examined the studies concerning the effects of metastatic lesions, the failure process, and the modeling of metastatically involved vertebrae.

We looked for evidences concerning the involvement in the failure process of location, dimension, and shape of a metastatic lesion. In the following, we will summarize the results of our research.

In an *in vitro* study (Silva, Hipp, McGowan, Takeuchi, & Hayes, 1993), Silva et al. analyzed the effects of defect location and defect size on the strength reduction of thoracic vertebrae. The study was performed on human vertebrae with simulated lytic metastases. According to the results, transcortical defects produced a significant reduction in the vertebral strength. However, the findings did not highlight a relation between the defect location and the strength reduction. The impact of the defect size on the strength reduction was found to be weak when the defect was transcortical.

Windhagen et al. conducted an *in vitro* study (Windhagen, Hipp, Silva, Lipson, & Hayes, 1997) on vertebrae with simulated lytic metastases in order to assess their absolute loadbearing capacity. In this study, defects (involving 5% to 20% of the volume of the vertebral centrum) were created in different location (i.e. posterior part, middle part, and lateral side). No correlation was found between failure load and defect size. The impact of location on the failure load was not assessed.

Whyne et al. performed an *in silico* study (Whyne, Hu, & Lotz, 2001) on the effects of tumor size, material properties, and compressive loading rate using a FEM of a lumbar

SMS³ (i.e. first lumbar vertebral body and adjacent discs). The tumor (25% or 50% defect of the trabecular bone by volume) was located in the center of the vertebral body. Vertebral body displacements and strains were highly affected by changings in tumor size, loading rates and trabecular bone density. Since the location was fixed, no remarks were made about its impact on vertebral strength.

Whyne et al. investigated the features that contribute to burst fracture risk in presence of spinal metastases (Whyne, Hu, & Lotz, 2003). They performed *in vitro* tests to validate a FEM. Tumor size, magnitude of loading, and bone density were discovered to be the principal factors leading to burst fracture. The FEM included a centrally located hemi-elliptical tumor (15%, 30%, and 45% defect of the trabecular bone by volume). The location influence on burst fracture risk was not assessed.

Tschirhart et al., in a FEA, studied the effects of tumor location and shape on vertebral body stability (Tschirhart, Nagpurkar, & Whyne, 2004). According to this study, the burst fracture risk was mainly influence by the tumor size. Tumor location was found to be relevant. If the tumor was located posteriorly, the vertebral bulge reached its' maximum. Lastly, tumor shape held a significant effect, with extended medio-lateral dimensions found to greatly increase the vertebral bulge.

Alkalay conducted a study on the failure process of human vertebrae (Alkalay, 2015). In his study, uncontained lytic defects (dimension equal to 40% of the vertebral body) were simulated in the body of osteoporotic vertebrae. Alkalay did not considered neither the lesion's location nor its' morphology.

In another study (Alkalay & Harrigan, 2016), Alkalay and Harrigan assessed the response of a QCT/FEM of a vertebra with simulated uncontained lytic metastases (involving 33% of the body). Again, location and morphology of the lesions accounted.

Palanca studied the effect on the superficial strain distribution of simulated bone metastases (Palanca, Barbanti-Bròdano, & Cristofolini, 2018). The study considered simulated lesions of different sizes (ranging from 10-20% up to 40-50% of the vertebral body), however it reported no evidence of an influence due to the lesions' position and morphology on the strain distribution.

³ A spinal motion segment (SMS) is a segment of spine composed by a vertebra and the two adjacent discs.

Recently, Costa performed a study (Costa, et al., 2019) on QCT/FEM of metastatically involved vertebrae (with lytic lesions), to assess the stability in case of an “indeterminate unstable” SINS. Information about the influence of morphology and location of the lesions were not provided.

In conclusion, the influence of defects’ shape and position within the verbal body is not well known. The relevant literature rarely focuses only on evaluating the influence of these parameters, and it is based either on *in silico* studies or on *in vitro* studies with simulated defects. To the author knowledge, studies that aim to assess the influence of these parameters on spine with actual metastases are still lacking.

1.5 The Aim of this Study

When reviewing the studies available, it is hard not to notice the general lack of interest towards the morphology of metastatic lesions.

Being tailored to clinicians' necessities, the clinical classification systems (e.g. SINS) overlook the mechanical aspect in its entirety. The subsequent evaluation lacks in mechanical evidence. While offering an insight over this deficiency falls beyond this work's aim, it is important to underline this shortcoming.

The literature concerning the position and the size of a lesion is scarce.

The works available generally do not focus solely on these two parameters.

In addition, to the author knowledge, the studies on the mechanical competence of metastatically involved vertebrae conducted are either *in vitro* with simulated lesions or *in silico*. Employment in an *in vitro* study of a vertebra with actual metastatic defects has yet to be performed.

Lastly, the authors generally attain different outcomes, which are often in disagreement. Given the background, the authors believe that further work is needed and that it must focus on assessing the role of defect position and shape.

In particular, the authors think that position and shape of the lesion might hold a key role for what concerns the risk of impending fracture in a metastatic spine.

The aim of this study is to study the mechanics of metastatically involved vertebrae.

Our purpose is to determine the influence of metastases' generated lesions on the superficial strains' distribution (obtained by means of DIC).

We also seek to assess the influence of three parameters on the strain distribution; these parameters being the type, the location, and the size of the metastasis.

We intend to design a versatile tool to assist in this endeavor.

Rather than being an exhaustive analysis of lesions' size and location effect on the strain distribution, this study is but a preliminary step to establish whether further research should strive to attain a deeper knowledge regarding the role of these parameters in spinal instability.

Chapter 2: Materials & Methods

2.1 Specimens

2.1.1 Specimens: Acquisition and Storage

Nineteen spine segments were obtained through an ethically approved donation program (AGR, Hanover, MD). The donors were male (8) and female (11), of Caucasian (17) and Black (2) ethnicity. The mean age was 70 year (range: 46-85; standard deviation: ± 13.21 year); the mean height was 177 cm (range: 152-185; standard deviation: ± 14.20 cm); the mean weight was 72 kg (range: 40-140; standard deviation: 29.59 kg); the mean body

ID	Segment	Cause of Death	Sex	Age	Ethnicity	h (cm)	w (kg)	BMI (kg/m ²)
766	T1-L3/4	Cancer w. Metastases	M	81	C	182	77	23
767	C1-S5	Respiratory Failure	M	63	C	185	79	23
768	L1-S5	Lung Cancer	F	85	C	152	38	16
769	C1-S5	Uterine Cancer	F	59	C	160	91	36
770	C1-S5	Lung Cancer	F	51	C	152	32	14
771	T1-L5	Bladder Cancer	M	75	C	172	49	17
772	T1-S5	Breast Cancer	F	82	C	157	54	22
773	T12-L5	Prostate Cancer	M	66	C	175	65	21
774	T4-S5	Breast Cancer	F	81	C	154	52	22
775	T1-S5	Breast Cancer	F	55	B	165	47	17
776	T1-S5	Prostate Cancer	M	83	C	175	64	21
777	T7-S5	Prostate Cancer	M	78	C	182	54	16
778	L1-S5	Adenocarcinoma	F	62	C	170	68	24
779	C1-S5	Breast Cancer	F	46	C	167	68	24
780	C1-S5	Breast Cancer	F	51	C	178	130	41
781	C1-S5	Lung Cancer	F	73	B	175	72	24
782	C1-S5	Adenocarcinoma	F	62	C	157	140	57
783	T12-L4	Lung Cancer	F	60	C	175	99	32
784	T2-T11	Prostate Cancer	M	52	C	172	50	17
785	C1-T12	Cancer w. Metastases	M	72	C	160	40	16

Table 1 - The table shows the spinal segments ID and the information available about the donors (included sex, age, ethnicity, height, weight, and body mass index).

mass index (BMI) was 25 kg/m² (range: 14-57; standard deviation: 10.72 kg/m²). The specimens ranged from full spines (C1-S5) to segments of five vertebrae.

The specimens were stored at -27°C, either in double plastic bags or wrapped in disposable surgical drapes and put in plastic bags.

2.1.2 Specimens: Clinical CT and Consultation

Each specimen was scanned using a clinical CT (Aquilion ONE, Toshiba, Tokyo, Japan) in a specialized facility⁴. The CT scanner was previously calibrated using a phantom (European Spine Phantom). The specifications of the scan were the following:

- Slice thickness: 1 mm;
- Pixel spacing: 0.251 mm, 0.251 mm.

An oncologist⁵ was consulted to assess the presence of metastases.

Being the primary imaging technique in the current clinical practice regarding cancer patients, clinical CT was chosen over other more detailed (and invasive) alternatives.

2.1.3 Specimens: Preparation and Alignment

From each specimen the soft tissues (ligaments, tendons, muscular fibers etc.) were removed, except for the intervertebral discs, which were kept intact.

The specimens were divided in segment of one to three complete vertebrae, depending on a series of parameters:

- For specimens where a metastatically involved vertebra was found near a healthy vertebra, the segment was composed of two complete vertebrae (mid segment), three discs, and two partial vertebrae (to physiologically transmit the load to the vertebra under investigation);
- For specimens where all the vertebrae were metastatically involved or a control was unavailable, the segment was composed of one complete vertebra, two adjacent discs, and two partial vertebrae;

⁴ Clinica Privata Villalba (Via di Roncrio 25, Bologna 40136, Italy)

⁵ Giovanni Barbanti-Bròdano, Department of Oncologic and Degenerative Spine Surgery, Rizzoli Orthopedic Institute (Via G.C. Pupilli 1, Bologna 40136, Italy).

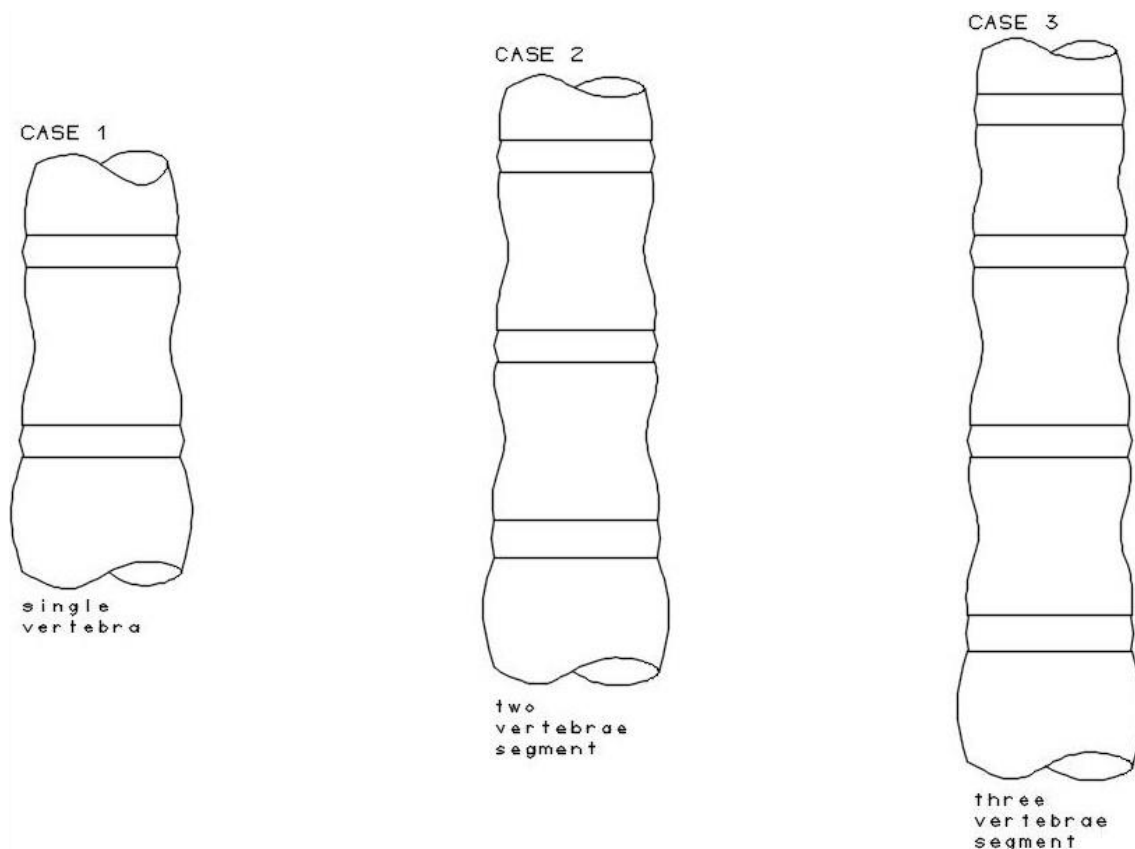


Figure 2 - Graphical representation realized via CAD of the three segments configuration. From left to right: two disc (single metastatic vertebra without control), three discs (metastatic vertebra with control), four discs (two metastatically involved vertebrae with control). The topmost and lowermost vertebrae were split to obtain two grips.

- In certain cases, a segment was made of three vertebrae (two metastatically involved and one healthy), their adjacent discs (five in total), and two partial vertebrae;

Once divided into segments, the cranio-caudal and right-left sizes were obtained for each tested vertebra using a caliper. The antero-posterior size was measured on the CT scans (OsiriX, Pixmeo, Bernex, Switzerland) (synedra View Personal, synedra IT, Innsbruck, Austria).

On the vertebral body, two marks were made, a cross frontally (corresponding to the point where craniocaudal and right-left sizes were half of their total value) and a straight line



Figure 3 - A three vertebrae segment (frontal view) mounted on the 6DOF clamp. Two crosslike marks are visible on the outermost complete vertebrae, the center is placed halfway the right-left and cranio-caudal lengths. These marks were used to align the specimen.

laterally (either on the left or right side, at half of the antero-posterior length). These marks were later used to align the specimen frontally (figure 5) and laterally.

Six wood screws were driven in the two partial vertebrae in order to increase the surface available to grip for bone cement. Three screws were placed on each of the two ends of the specimen.

The specimen was then aligned using a 6 DOF clamp. The specimen was firstly aligned frontally and then laterally using an engineer's square as reference.

A metal pot was placed under the specimen, with its center corresponding to the projection of the center of the specimen⁶ on its surface.

⁶ The center of the specimen depended on the segment type (one vertebra, two or three vertebrae). These "centers" were defined accordingly:

- For a specimen with one tested vertebra, the center of the specimen corresponded to the center of the vertebral body;
- For a specimen with two tested vertebrae, the center of the specimen corresponded to the center of the disc between them;
- For a specimen with three tested vertebrae, the center of the specimen was midway on the straight line connecting the centers of the two outermost vertebrae.

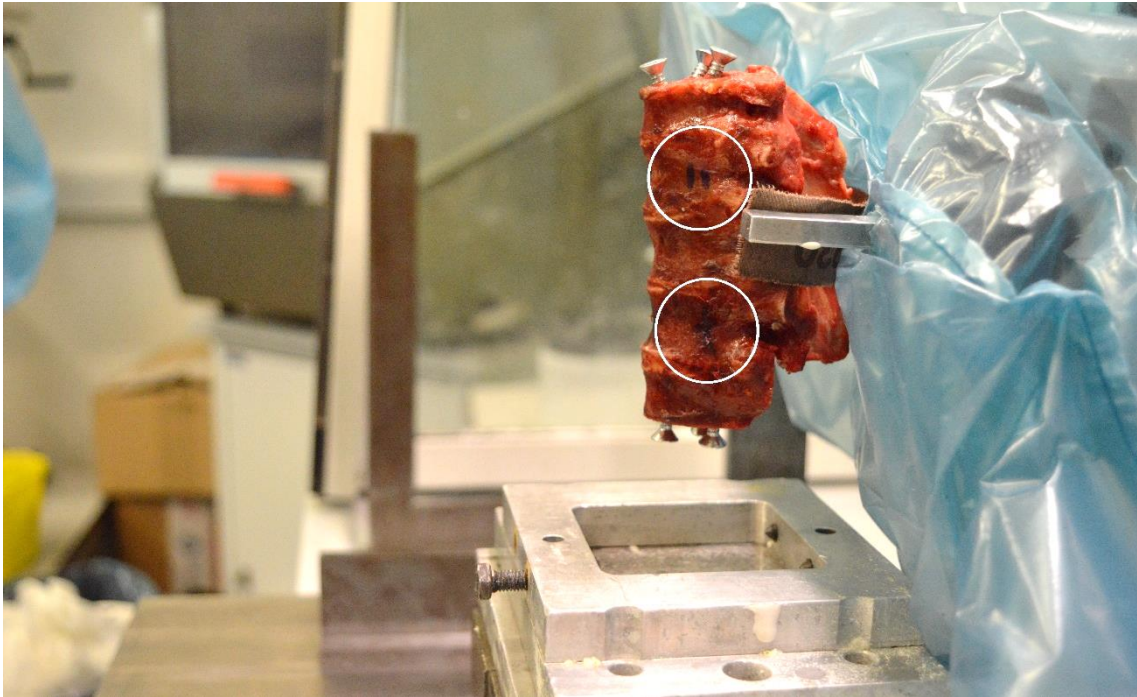


Figure 4 - A three vertebrae segment (lateral view). A straight mark is visible on the surface of each of the two outmost vertebrae. The mark corresponds to half of the antero-posterior length of the relative vertebrae. These marks were used to align the specimen.

Once alignment was completed, the specimen's lower end was inserted into the pot cavity. Bone cement was prepared using polymethyl methacrylate (PMMA) powder (supplied by Tecres, Sommacampagna, VR, Italy) and a monomer, in a ratio of 2:1. Following its

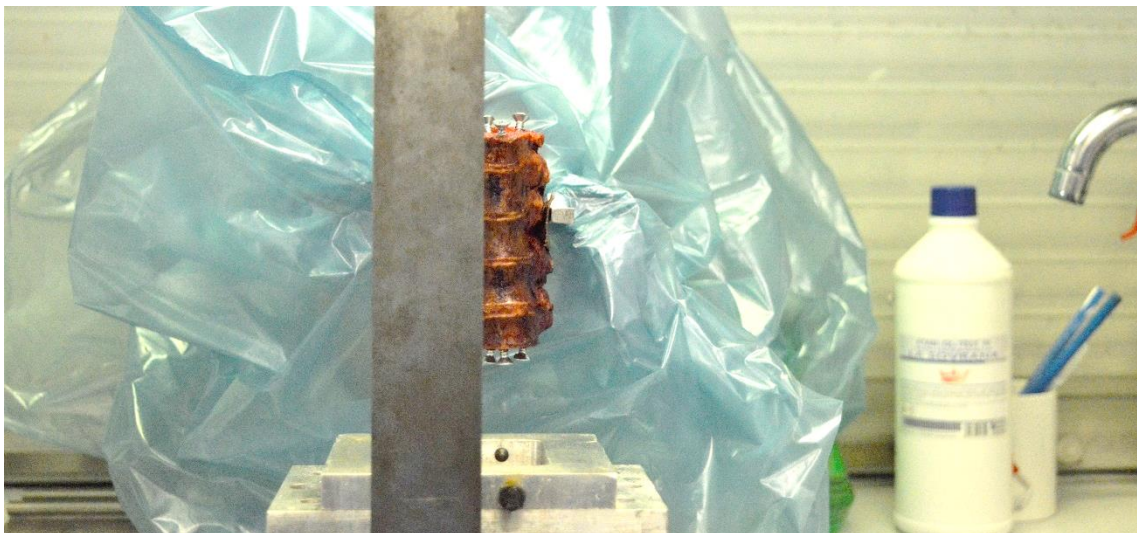


Figure 5 - Frontal alignment of a three vertebrae segment. The crossess' centers were aligned by eye with the aid of a engineer's square.



Figure 6 – Alignment of the pots performed with the aid of two engineer's squares, prior to cementation.

preparation, the bone cement was poured into the pot and left to stir at room temperature (24°C) until there were no signs of viscous PMMA gel.

The specimen was rotated upside down and a second pot placed under its free end. The two pots were aligned using two engineer's squares. The specimen's lower end was placed within the pot cavity and fixed using bone cement.

2.2 Digital Image Correlation (DIC)

In order to measure the field of strain on the surface of the vertebral body, three-dimensional digital image correlation (DIC) was employed.

The concept of “three-dimensional” should not be misinterpreted. 3D does not stand for a volumetric analysis of the specimen, which is conducted via DVC (digital volume correlation). DIC, both in its 2D and 3D implementations, measures the field of displacement (and strain) on a surface. The difference between these two methods lies in how they are implemented. 2D-DIC uses one camera, perpendicular to the surface investigated, and measures only the displacements and the strains on a plane. 3D-DIC implements two cameras and exploits the stereoscopic vision to acquire the displacements both on and out of the acquired plane.

2.2.1 DIC: A General Overview

DIC allows the measurement of the displacement and strain fields of a surface.

To operate, DIC requires a series of images of the investigated surface, in its original state and under deformation. The sequence of images is acquired using a sensor (i.e. a digital camera). A software compares the images and computes the displacements on the surface (and, by derivation, the strains).

The tested surface must present a specific random pattern in order to observe how it displaces under a certain loading configuration. The pattern allows the univocal identification of the regions on the specimen.

If the specimen does not feature a similar pattern, it must be painted on its surface. This pattern should be a high-contrast black-on-white or white-on-black speckle pattern, as it reduces the effect of the noise (Cristofolini, 2015, p. 192) and takes full advantage of the DIC’s cameras (which are often black-and-white, to minimize the noise). When creating a pattern, the paint should displace and strain with the specimen without crumbling or cracking. Moreover, the paint should not change the specimen’s mechanical properties.

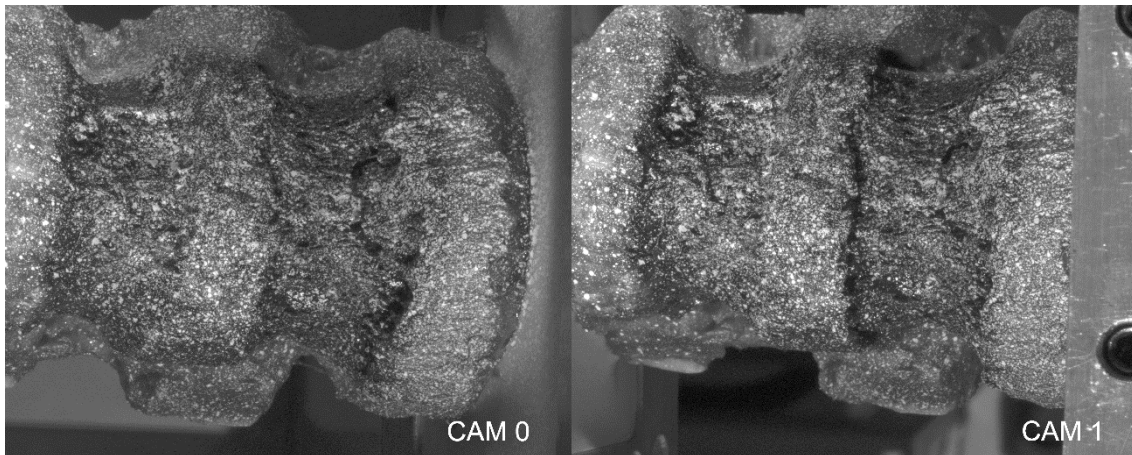


Figure 7 - A pair of images acquired by two DIC cams in a 3D implementation.

The speckle pattern can be painted using an airbrush gun or a paint can. Toner powder is another viable solution, though its disadvantages are something to be dealt with⁷.

For what concerns the sensor and the operating principle, there are two implementations of the DIC: 2D and 3D.

2D-DIC employs a single camera (sensor) to measure the field of displacement on a surface.

3D-DIC (which is the implementation of DIC used for this study) employs two digital cameras to acquire a stereovision⁸ of a single surface three-dimensionally.

In order to operate correctly, the two cameras must be synchronized (i.e. the acquisition of two different views of the surface must be simultaneous) and sufficiently distant (Cristofolini, 2015, p. 199).

From the simultaneously acquired images, the position of any point on the targeted surface can be triangulated. The triangulation process requires two inputs: the coordinates of the target on the image planes and the parameters of the system, internal (e.g. focal

⁷ While toner powder allows to control the size of the dots, its dots displace but do not strain with the material. This constitutes the major drawback of toner powder (Cristofolini, 2015, p. 192).

⁸ Stereoscopic vision is the ability to perceive an object as three-dimensional. In order to perceive the depth of a target, it must be observed at least from two points of view (not superimposed). In the human being, stereoscopic vision is achieved using a pair of eyes. In DIC, the combined use of two cameras allows to achieve stereoscopic vision.

length, lens distortion, principal point) and external (e.g. position of the camera). The formers are known, the latter are obtained *via* calibration⁹.

2.2.2 DIC: Considerations on the Set-up

When operating DIC, a suitable lighting must be arranged. If the testing environment cannot provide a stable and adequate illumination, additional light sources must be used. These light sources are generally high-power LEDs (either white or green).

The need for additional light sources is linked to the camera lenses and their settings. If the light is insufficient, the operator must compensate with a wide range of aperture (small f-number) or with a long shutter time. A small f-number results in blurry images and in short depth of field. A long shutter time exposes to motion blur. Either way, the resulting image will be deteriorated.

Another problem regarding the lenses must be addressed. The lenses can be wide-angle, long-focus, or telecentric. Wide-angle lenses allow for a larger field of view (FOV), but the resulting image is often highly distorted (thus increasing the risk for computational errors). Long-focus lenses can be placed at a larger distance, with a resulting increase in the FOV. Telecentric lenses collect an image with the same size of the lens itself (therefore the distortion is minimal); however, these lenses are expensive, and they might be unsuitable for large specimen.

A specific problem associated with 3D-DIC is the angle between the two cameras. If the angle is increased, the esteem of the displacement in the third dimension (i.e. inward and outward the surface) is more accurate; nevertheless, some areas might not correlate with large angles¹⁰. Reasonably, the angle between the two cameras should be of 20-25°.

⁹ Calibration is a procedure to calculate the parameters of a certain system. It involves the acquisition a target of known coordinates (i.e. a calibration target) in different poses within a certain volume (i.e. calibrated volume). These acquisition are used as input for the minimization of a cost function, whose outputs are the system parameter (Cristofolini, 2015, p. 199).

¹⁰ This occurs because a portion might be seen by one camera while being hidden to the other (which has a different point of view on the specimen). In addition, a same segment, depending on its position, might be highly distorted in one of the two images.

2.2.3 DIC: The Digital Noise

Since strains are obtained by mean of derivation, and derivation enhances the noise, it is important to know the nature of the noise afflicting a digital image in order to prevent it or, otherwise, to filter it.

Noise can afflict both the acquisition and the processing. The error afflicting a digital acquisition (be it an image or a measurement) can be either systematic or random.

Regarding the sensor, the main systematic error afflicting an image is associated to the different gain of each pixel on CCD sensor¹¹, however small. Random noises are associated with the detection of photons (i.e. the variation in the number of photons detected in contiguous frames of time), the thermal vibration (i.e. the generations of electrons due to physical processes, not the photon absorption), and the excess noise (i.e. noise with a pink wavelength that causes the memory to deviate from a zero average).

Some errors can be attenuated (e.g. cooling down the sensor to reduce thermal vibration or filtering a signal to lower the excess noise), others cannot be reduced.

Systematic and random errors are associated with the phase of signal processing. These errors propagate to the computation of the displacement. Random noise is amplified when computing the strains, because of the derivation process.

2.2.4 DIC: The Set-up for this Study

A set-up similar to the one used by Palanca in previous studies (Palanca, Barbanti-Bròdano, & Cristofolini, 2018, p. 111005(3)) (Palanca, Marco, Ruspi, & Cristofolini, 2018, p. 77-78) was used.

We used a commercial 3D-DIC system (Q400, Dantec Dynamics, Skovlunde, Denmark). The sets of images were acquired by two black-and-white cameras (5 MP, 2400×2050, 8b) with high-quality metrology-standard 35mm lens (Apo-Xenoplan 1.8/35, Schneider-Kreuznach, Bad Kreuznach, Germany; 135mm equivalent).

¹¹ Two are the main technologies employed in digital camera sensors: CCD (charge-coupled device) and CMOS (complementary metal-oxide semiconductor). In general, CCD sensors allow to acquire an image having both a higher quality and lower noise than those operating *via* CMOS. DIC cams usually use CCD sensor, thus, when speaking of camera related problems, we will imply that they use CCD technology.

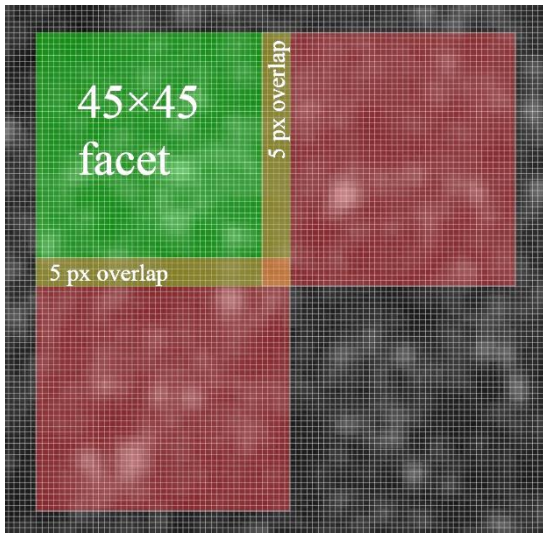


Figure 9 - Detail of the white-on-black pattern of a tested specimen. Three 45x45 facets are highlighted. A 5 px overlap is set to provide a certain degree of redundancy (thus, a better estimate of the displacements). The image was acquired with a DIC camera.

Spatial resolution was estimated to be better than 3 mm. The nonlinearity of the correlation and the smoothing process prevented to give an exact quantification of the value.

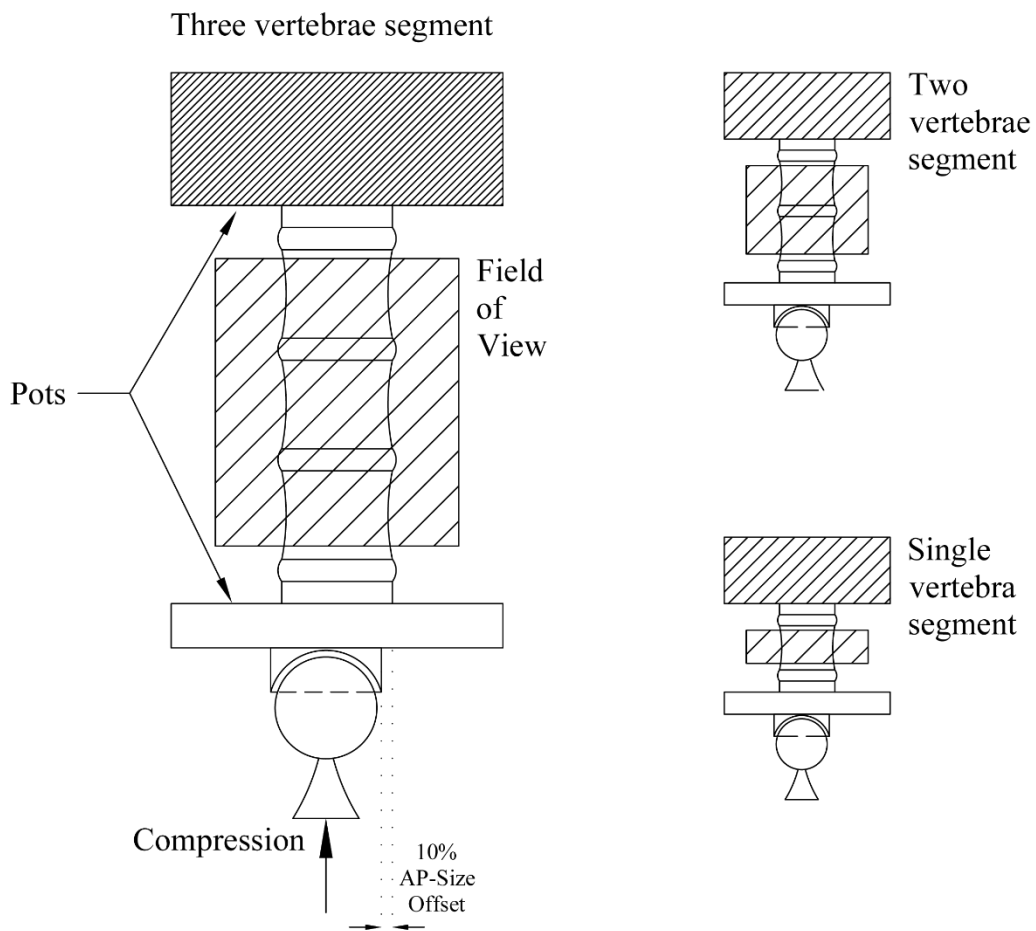


Figure 10 - Field of view (FOV) for each of three types of segment.

2.3 Test

2.3.1 Test: Surface Preparation

On the day of the test, the specimens were removed from the freezers.

To perform the DIC test, a high-contrast white-on-black pattern was created on the studied surface of the specimen. A dark stain (a saturated solution of water and methylene blue) was applied on the surface of the vertebral body and the discs between the tested vertebrae. A random white speckle pattern was formed by spraying at 300 mm from the specimen with either an airbrush (AZ3 HTE 2, nozzle 1.8mm, Anest Iwata, Varese, Italy) or a paint can.

A water-based paint (Q250201 Bianco Opaco, Chrèon, Como, Italy) diluted at 40% was used with an optimized setting for the pattern (air pressure: 100kPa) to not perturb the mechanical properties of the specimens.

The specimen was subsequently fixed to two metal pots. A hemispherical socket was put to the lower pot (i.e. the one to whom the cranial end was secured). The socket's position



Figure 11 - White speckle pattern on a methylene blue background, dyed on the surface of the specimen.

was fixed with an anterior offset from the center equal to the 10% of the antero-posterior size of the metastatic vertebra.

2.3.2 Test: Set-up Adjustment

Once ready, the specimen was mounted on the testing machine (testing system: 8032, Instron, Cambridge, UK; loading cell: 100 kN, Instron; controller: 8800, Instron). The specimen cranial end was connected to the actuator (a ball joint) in order to emulate the physiological loading transmission¹².

The movement of the low friction linear bearings was limited to reduce the out-of-plane movement of the specimen.

DIC cameras were positioned in front of the specimen. The focus was regulated manually until the speckle patterned reached the optimal sharpness.

The system was calibrated using an aluminum target.

Two images of the surface of the specimen were acquired without any load. This allowed to evaluate the minimum systematic and random errors in a zero-strain condition.

Prior to test, preconditioning (20 cycles, haversine, 0.5 mm displacement, 1 Hz) was performed to reduce the effects of viscoelasticity and to allow the testing setup to settle.



Figure 12 – Instron 8032, the servo hydraulic system employed to test the specimens.

¹² Loads in the human spine are transmitted from the top to the bottom. The loads experienced by the human vertebrae are for the most part compressive. This is shown by the distribution of the trabeculae in the cancellous bone (aligned with the axial forces).

Testing Machine Layout

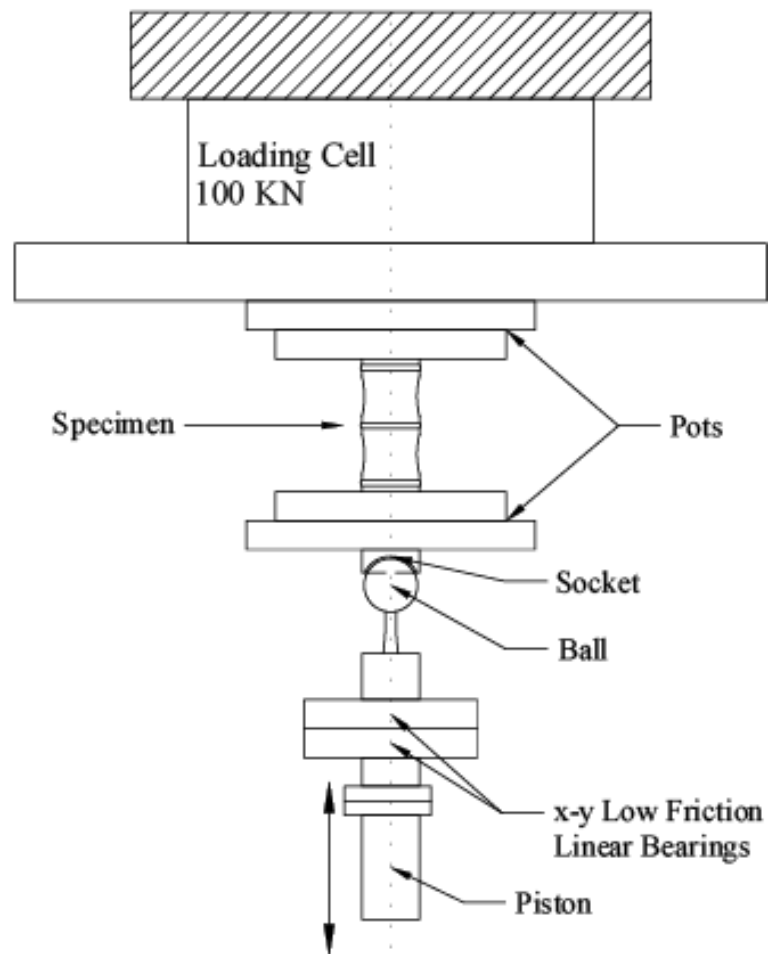


Figure 13 - Testing machine layout. Only compressive loads were studied; the movement of the linear bearings was limited to prevent unwanted loading components.

2.3.3 Test: Test Design

The specimens were tested with a combination of compression and anterior bending. The resulting system was statically indeterminate¹³, hence far from a physiological

¹³ A statically indeterminate (or hyperstatic) condition occurs when the equation for static equilibrium are insufficient to determine the internal forces and the reactions acting on a constrained structure. This condition pertains completely constrained structures where DOF are redundantly interdicted.

The deformations must be considered to solve a statically indeterminate system.

In our case, two constraints were imposed to the specimens (6DOF). The uppermost constraint blocked 6 DOF. The lowermost constraint blocked 4 DOF, while allowing translation longitudinally and out-of-the-plane (although to a limited extent).

configuration (the emulation of physiological loading condition was not our main concern).

The specimens were tested with progressive load limits, in order to perform a step by step assessment of the field of strain while avoiding damages to the specimen (being the test non-disruptive).

The limits defined were 0.5BW, 1BW, and 1.5BW.

2.3.4 Test: Mechanical Testing

The test was carried out imposing a displacement equivalent to 0.5BW per 1 Hz (waveform: single ramp). The magnitude of the displacement to be imposed was assessed prior to test by reaching manually a compression of 0.5 BW.

A first acquisition was performed for each specimen with the former displacement and by limiting the load to 0.5BW.

Correlation was performed and the resulting field of strain evaluated. If the superficial strains weren't suggesting an impending risk of fracture, a new test was performed.

The second acquisition was carried out imposing the same displacement and by changing the limit to 1BW.

A similar assessment was made on the resulting field of strain, and, in case, a third test with a new limit of 1.5BW was executed.

In certain cases, if the strains at 0.5BW were suggesting a significant risk of fracture, a second test (same displacement, limit at 0.75BW) was designed to be carried out.

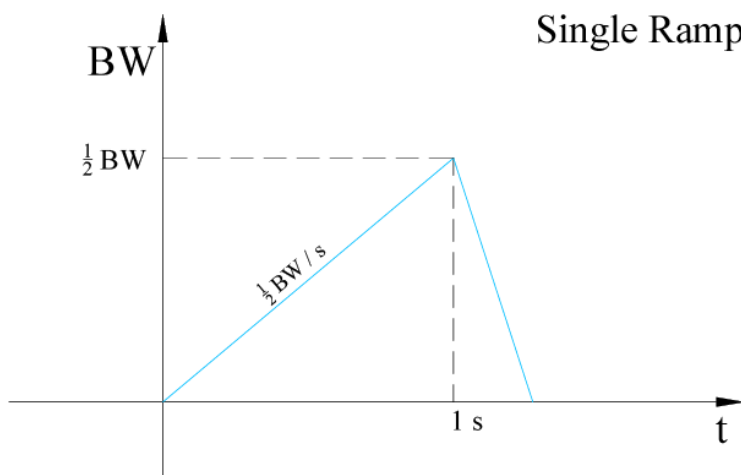


Figure 14 - Example of the waveform employed for the mechanical testing of the specimens. The test was carried out by imposing a displacement equivalent to half body weight per hertz.

2.4 Assessment of the Position and Size of the Metastases

Our goal was to realize a versatile tool to perform an explorative analysis for researchers in spine biomechanics.

Each vertebra was divided in three section, in each section the lesions were located using a custom mask.

A simplified geometric model was designed for lytic lesions.

Location and geometric “modelization” were performed only on the most significant lytic lesions. This was made on the assumption that greater lesions would likely have a greater impact on the strain distribution.

Blastic lesions were accounted only during the analysis, not when creating the model.

2.4.1 Assessment of the Position and Size of the Metastases: The Mask

For each of the available spine, we identified the metastatic vertebrae.

For each metastatic vertebra, in multiplanar reconstruction, we measured the cranio-caudal size (defined as the distance between two endplates, obtained from the center of

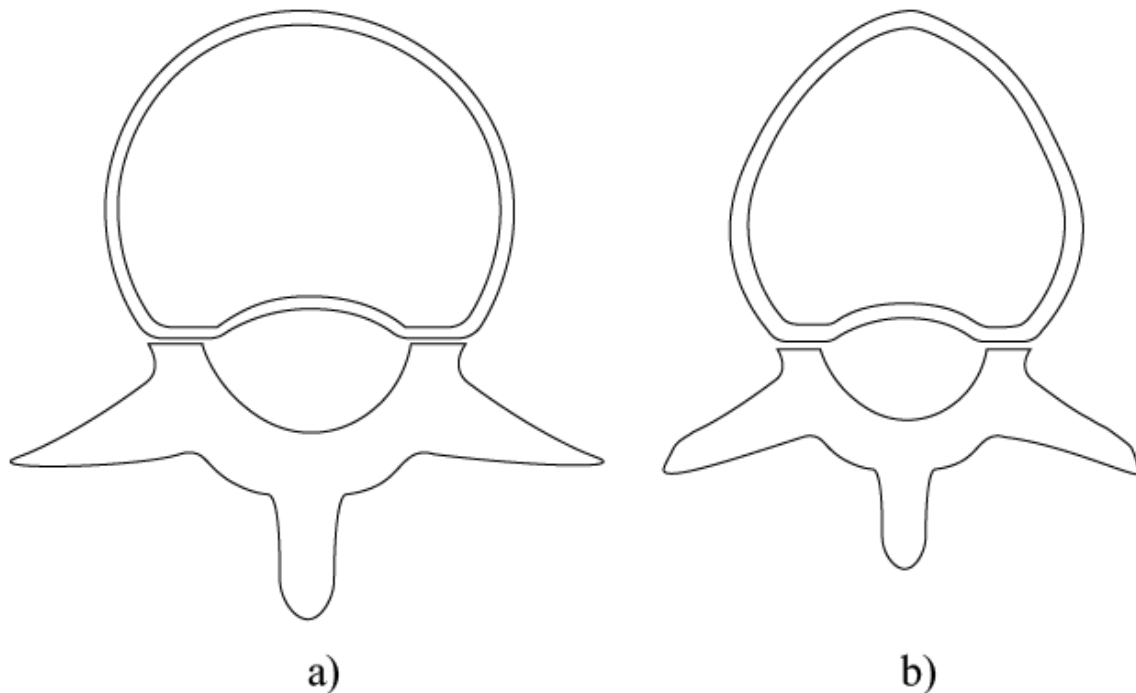


Figure 15 - Conceptualized lumbar (a) and thoracic (b) vertebrae.

the vertebral body) using the viewers' built-in tools (i.e. measure distance). The measurements were taken on the frontal plane, with the cursor centered on the vertebral body.

Each vertebra was divided in three sections. Each section measured longitudinally a third of the cranio-caudal size. The sections were named after their position: superior, central, and inferior. A "sample" of the vertebral transverse plane was taken at half of the section *circa*.

On a CAD software (AutoCAD, Autodesk, San Raphael, CA), a custom mask was built and superimposed on the "samples".

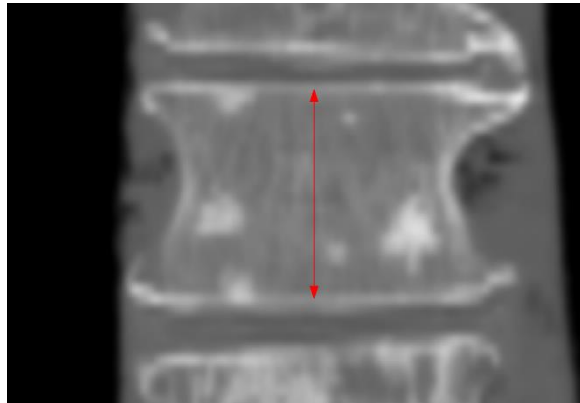


Figure 16 - Cranio-caudal size (the red line in figure) was obtained by measuring the distance between the endplates (portions of the vertebral body which interface with the intervertebral discs). Being made of cortical bone, the endplates can be recognized by their light color (high density).

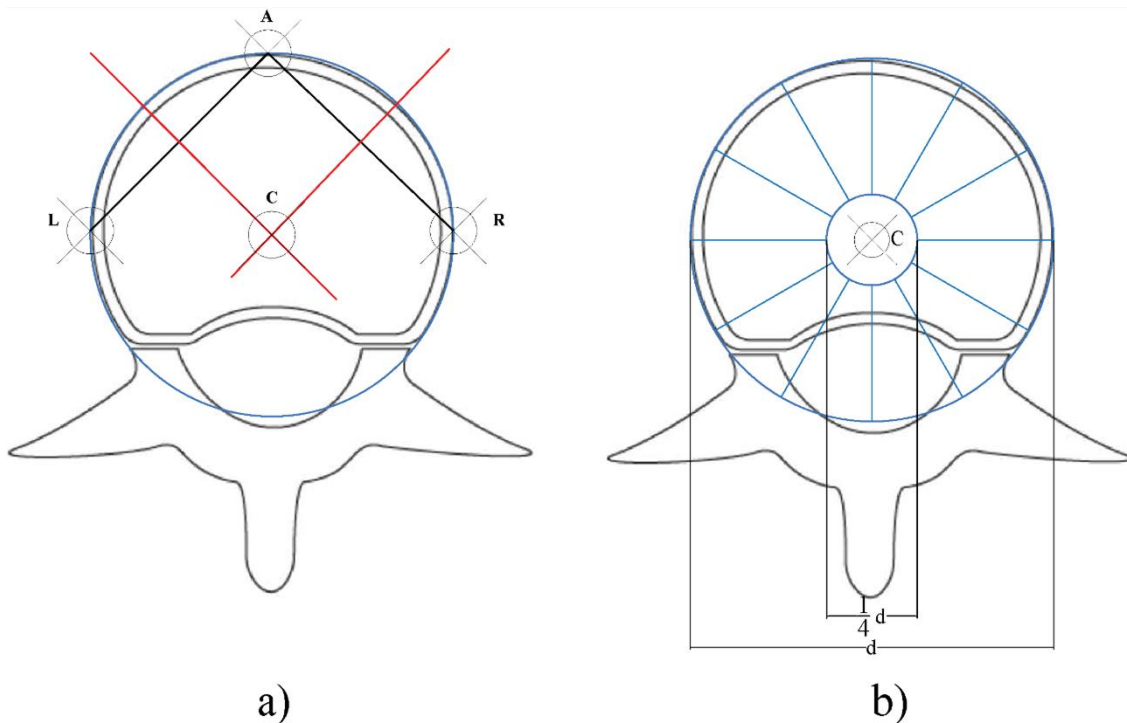


Figure 17 - Identification of the three reference points for the creation of the outermost circle (a) and the final clock-like mask (b) on the conceptualized lumbar vertebra.

Using the Weinstein-Boriani-Biagini system (Hart, Boriani, Biagini, Currier, & Weinstein, 1997) as reference, the mask was designed to resemble a clock (with the right side of the vertebra corresponding to the hours from twelve to six o'clock). The clock was constituted of two concentric circles. The outermost circle was built using three reference points. These points were identified as the right-most, left-most and most anterior points on the vertebral body surface. The innermost circle (named *nucleus*) was designed to have a diameter equal to a quarter of the outermost's.

The outermost circle was divided in 12 circular arcs measuring 30 degrees. Each circular arc was identified by a number from one to twelve (clockwise increment).

The *nucleus* was left undivided, and it was identified by the letter N.

We identified a total of 39 regions (36 circular arcs and 3 *nuclei*) for each vertebra.

The position of the lesions on the mask (subsequently, on the metastatic vertebra itself) was expressed through a Boolean. The value of "true" was associated with the presence of metastases in a region. *Vice versa*, the value "false" was assigned to the regions without metastases. Graphically, the presence of a metastasis was represented by filling the region with a pattern.

2.4.2 Assessment of the Position and Size of the Metastases: Tests for the Intra-Operator Repeatability

Intra-operator repeatability was tested for the joint processes of samples' acquisition and lesion's identification, and for the process of lesion's identification only.

In the former case, the process was repeated in its entirety, from the acquisition of the sample on the CT-scans to the identification of the lesions within the vertebral body.

In the latter case, three samples for each vertebra were acquired only the first time. Only mask's creation and lesion's identification were repeated on each session of testing.

In both cases, the tests were carried out in three different times on three vertebrae with different lesions (i.e. mixed, lytic only and lytic with capsule) by one operator.

We preferred to give a qualitative assessment of the intra-operator repeatability.

2.4.3 Assessment of the Position and Size of the Metastases: Tests for the Inter-Operator Repeatability

To test inter-operator repeatability, three vertebrae with different lesions (i.e. mixed, lytic only and lytic with capsule) were analyzed by four operators.

Three samples were obtained from each vertebra at the defined position (i.e. inferior, central, and superior). On each sample the mask was superimposed.

Each of the operators was tasked to autonomously analyze the samples and to locate the metastases.

2.4.5 Assessment of the Position and Size of the Metastases: Assessing Lytic Metastases Size

A simple geometric model was created to obtain an estimate of the analyzed lesions' size. An accurate description of the lesioned volume was not among this study aim. For a more accurate analysis, bone densitometry¹⁴ should be performed.

Lytic lesions were described as spheres. The diameter of the sphere was obtained by measuring (on the CT scans *via* viewer's built-in tools) the maximum size of the metastasis on the transversal plane of the VB. The lesion volume was then calculated and normalized to the volume of the modelled vertebra (a cylinder with a height equal to the cranio-caudal size, and a diameter equal to the right-left size).

2.4.6 Assessment of the position and size of the Metastases: Application of Mask and Model

As previously stated, the main objective of this tool was to describe osteolytic lesions within the vertebral body both qualitatively (location of the lesion) and quantitatively (size of the lesion).

The masks were applied only on vertebrae with lytic or mixed metastases.

In case of mixed metastases, the masks were employed only to determine the location of lytic lesions.

¹⁴ Also called dual-energy x-ray absorptiometry (DEXA). It allows for a measurement of the bone mineral density (BMD). To perform this measurement, a small dose of ionizing radiation is used, as it allows to obtain a map of the internal structure of the bone.

Blastic lesions (be they in a vertebra with mixed or homogeneous metastases) were not located. Nevertheless, their presence was taken into account when the results of the mechanical tests were analyzed.

2.5 Metric

From the compressive test of the segments and the use of 3D-DIC, we obtained a 3D reconstruction of the field of strain distribution.

We focused our analysis on the study of engineering principal strains (eps), both maximum (eps1) and minimum (eps2).

The field of strain was analyzed quantitatively in specific regions of interest (ROI) for eps1 and eps2. In each ROI, the maximum, minimum and mean (with standard deviation) strain values were computed.

If a control was available, the normalized mean strain value (NMSV) was computed. NMSV was defined as:

$$NMSV = \frac{Metastasis\ MSV}{Control\ MSV}$$

With the aid of the mask and the geometric model, we located the most significant lytic lesions within the vertebral body and obtained a first estimate of their dimensions.

This information was later used for a qualitative analysis.

The qualitative analysis involved the search by eye of a correlation between the strain field and the lesions' type, location and size.

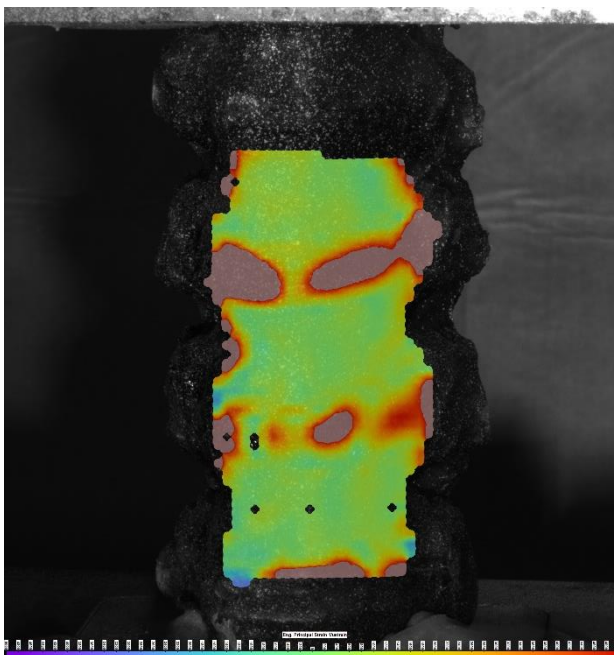


Figure 18 - Example of the strain field distribution (view as eps1) obtained via DIC. Green correspond to a zero strain condition, violet to a condition of compression, red to stretch.

Chapter 3: Results¹⁵

3.1 Quantitative and Qualitative Analysis

Of the nineteen spines available, five were prepared. From these, we obtained eight specimens of various length: two discs segments (2), three discs segments (4), and four discs segments (2).

The following operations were performed on each of the resulting segments:

- Determination of maximum, minimum and mean strain value in regions of interest (ROI);
- Location of lytic lesions by mean of the mask;
- Computation of an estimate for the volume of lytic lesions.

Patient ID	Segment	Specimens Obtained	Vertebra w. Metastasis	Type of Metastasis
773	T12-L5	L1 1/2 - L3 1/2	L2	Osteoblastic
		L3 1/2 - L5 1/2	L4	Osteoblastic
775	T1-S5	T12 1/2 - L3 1/2	L2	Osteolytic
		T9 1/2 - T12 1/2	T11	Osteolytic
779	C1-S5	T2 1/2 - T6 1/2	T4	Osteolytic
			T5	Osteolytic w. Capsule
		T7 1/2 - T10 1/2	T8	Mixed
784	T2-T11	T6 1/2 - T9 1/2	T8	Mixed
785	C1-T12	T4 1/2 - T8 1/2	T5	Osteolytic
			T6	Osteolytic

Table 2 - Specimens obtained from each of the prepared spinal segments.

¹⁵ Quantitative analysis of the strain field distribution was obtained from the work of Mara Marciante
Invalid source specified..

3.1.1 Qualitative and Qualitative Analyses: Specimen 773

Specimen 773 was divided in two segments of two discs.

In both segments, the tested vertebrae were involved with osteoblastic lesions. A control was not available for neither the first nor the second segment.

Being involved only with blastic lesions, masks were not built for the tested vertebrae.

Eps1 and eps2 computed for the segment L1½-L3½ (figure 19 and 20) can be found on the table 3. For segment L3½-L5½ (figure 21 and 22), eps1 and eps2 can be found on table 4. For sake of conciseness, we will not report them here.

Specimen 773 - Segment L1½-L3½

Engineering Principal Strain 1			
Load	0.5 BW	1 BW	1.5 BW
Mean (\pm SD) [$\mu\epsilon$]	40 (\pm 110)	600 (\pm 130)	7100 (\pm 300)
Minimum [$\mu\epsilon$]	-8654	-2252	-6295
Maximum [$\mu\epsilon$]	13334	52207	39383

Table 3 - The table shows the mean value, the maximum, and the minimum eps (both 1 and 2) for vertebra L2 (specimen 773) in the ROI.

Engineering Principal Strain 2			
Load	0.5 BW	1 BW	1.5 BW
Mean (\pm SD) [$\mu\epsilon$]	-180 (\pm 90)	-2760 (\pm 130)	-4000 (\pm 200)
Minimum [$\mu\epsilon$]	-36339	-45504	-49787
Maximum [$\mu\epsilon$]	473	984	16457

Specimen 773 - Segment L3½-L5½

Engineering Principal Strain 1			
Load	0.5 BW	1 BW	1.5 BW
Mean (\pm SD) [$\mu\epsilon$]	50 (\pm 110)	40 (\pm 120)	-50 (\pm 140)
Minimum [$\mu\epsilon$]	-1994	-1767	-5257
Maximum [$\mu\epsilon$]	8979	9850	28599

Table 4 - The table shows the mean value, the maximum, and the minimum eps (both 1 and 2) for vertebra L4 (specimen 773) in the ROI.

Engineering Principal Strain 2			
Load	0.5 BW	1 BW	1.5 BW
Mean (\pm SD) [$\mu\epsilon$]	-180 (\pm 90)	-2760 (\pm 130)	-380 (\pm 160)
Minimum [$\mu\epsilon$]	-14087	-6390	-4138
Maximum [$\mu\epsilon$]	1095	1097	1905

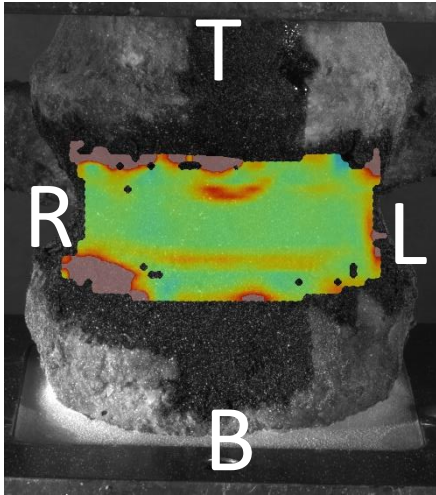


Figure 19 – Maximum eps (ϵ_1) for vertebrae L2 under a load of 1.5BW. The strain field appears homogenous. The strains are modest and the only notable peaks are in proximity of the intervertebral discs.

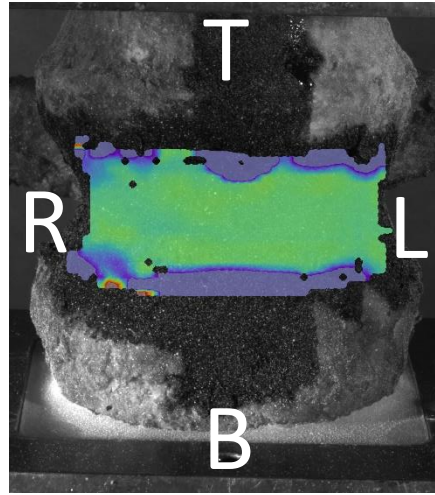


Figure 20 – Minimum eps (ϵ_2) for vertebrae L2 under a load of 1.5BW. As previously noticed, the strain field appears homogenous.

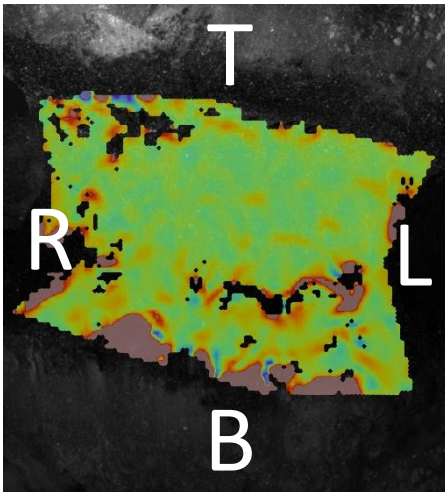


Figure 21 – Maximum eps (ϵ_1) for vertebrae L4 under a load of 1.5BW. The strain field is nearly homogenous. The strains are modest. Peaks are found in proximity of the intervertebral discs and near uncorellated zones.

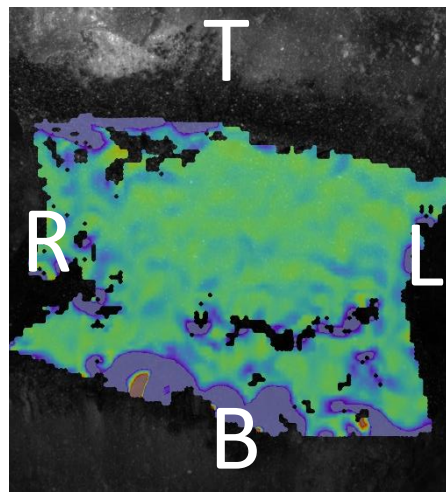


Figure 22 – Minimum eps (ϵ_2) for vertebrae L4 under a load of 1.5BW. As before, the strain field appears homogenous, except for strains near uncorellated zones.

3.1.2 Qualitative and Qualitative Analyses: Specimen 775

Two segments of three intervertebral discs were obtained from specimen 775.

The first segment, from T9½-T12½, was composed of a metastatically involved vertebra (T11) and a control (T10). The studied vertebra was involved with lytic lesions.

Lytic lesions were found in the central section, both anteriorly and posteriorly on the vertebral body (figure 23).

A maximum load of 0.75BW was chose to avoid any risk of fracture.

Since a control was available, the mean value of the strains on the metastatically involved vertebra was normalized to the value on the control vertebra. Under a load of 0.5BW, the normalized strain value was -2.97 for maximum eps and 6.38 for minimum eps; while, under a load of 0.75BW, we found the normalized strain value to be 1.13 (ϵ_1) and 3.67 (ϵ_2).

Compared to the masks, the lesioned vertebrae showed little to no anomalous strain when maximum eps were analyzed. Small areas with strain peaks were located anteriorly, between the central and inferior sections, in proximity to one of the regions designated as metastatic.

When minimum eps were considered, significant peaks were found between the central and inferior part of the vertebral body. These peaks, spanning from left to right, were located slightly under the central part of the vertebral body, near both to non-metastatic and metastatic areas of the central section.

The second segment obtained from 775 was composed of the vertebrae from T12½-L3½. The segment was composed of both a metastatic vertebra (L2) and a healthy one (L1). Lytic lesions were found in the metastatic vertebra.

The lesions were found posteriorly in the central section, on the right side of the vertebral body (figure 26). The mask was only partially built for the superior part of the vertebra since it was collapsed.

The normalized strain mean value for the maximum eps was -0.67 (0.5BW), 3.25 (1BW), and 5 (1.5BW). For the minimum eps, the normalized strain mean value was 1.46 (0.5BW), 0.63 (1BW), and 1.01 (1.5BW).

No notable match between the location of the lesions and the field of strain was found.

When minimum eps were considered, a peak in compression could be detected on the right side of the segment. Yet, being these strains near the boundaries of the mask (and being the boundaries often noisy), it could not be related to the position of the metastasis.

Specimen 775 - Segment T10^{1/2}- T12^{1/2}

Engineering Principal Strain 1				
Load	0.5 BW		0.75 BW	
Vertebra	T11	T12	T11	T12
Mean (\pm SD) [$\mu\epsilon$]	300 (\pm 200)	-890 (\pm 150)	900 (\pm 200)	1020 (\pm 110)
Minimum [$\mu\epsilon$]	-2313	-2879	-3885	-3051
Maximum [$\mu\epsilon$]	5672	8360	11789	12000

Engineering Principal Strain 2				
Load	0.5 BW		0.75 BW	
Vertebra	T11	T12	T11	T12
Mean (\pm SD) [$\mu\epsilon$]	-1410 (\pm 190)	-8990 (\pm 180)	-2600 (\pm 200)	-9530 (\pm 200)
Minimum [$\mu\epsilon$]	-5817	-67628	-13323	-88044
Maximum [$\mu\epsilon$]	-116	769	-198	736

Table 5 - The table shows the mean value, the maximum, and the minimum eps (both 1 and 2) for vertebrae T11 and T12 (specimen 775) in the ROI.

Specimen 775 - Segment T12^{1/2}-L3^{1/2}

Engineering Principal Strain 1						
Load	0.5 BW		1 BW		1.5 BW	
Vertebra	L1	L2	L1	L2	L1	L2
Mean (\pm SD) [$\mu\epsilon$]	-30 (\pm 70)	20 (\pm 90)	80 (\pm 80)	260 (\pm 110)	90 (\pm 90)	450 (\pm 120)
Minimum [$\mu\epsilon$]	-525	-870	-323	-559	-592	-1406
Maximum [$\mu\epsilon$]	1357	3417	1080	620	3289	11152

Engineering Principal Strain 2						
Load	0.5 BW		1 BW		1.5 BW	
Vertebra	L1	L2	L1	L2	L1	L2
Mean (\pm SD) [$\mu\epsilon$]	-390 (\pm 50)	-570 (\pm 100)	-480 (\pm 70)	-300 (\pm 130)	-680 (\pm 70)	-690 (\pm 140)
Minimum [$\mu\epsilon$]	-12139	-19311	-1260	-2936	-30211	-39828
Maximum [$\mu\epsilon$]	18	398	-71	337	270	1124

Table 6 - The table shows the mean value, the maximum, and the minimum eps (both 1 and 2) for vertebrae L1 and L2 (specimen 775) in the ROI.

Vertebra: T11
Specimen: 775

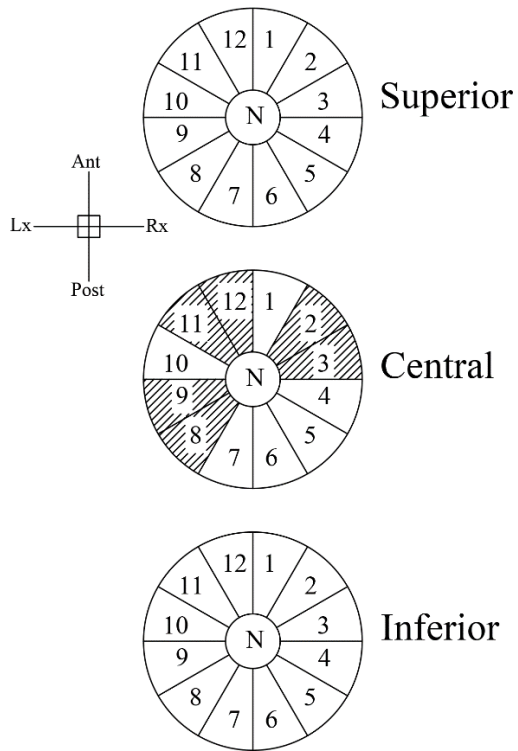


Figure 23 - Masks for vertebra T11 (#775). Lytic lesions were found in the central section, both anteriorly and posteriorly.

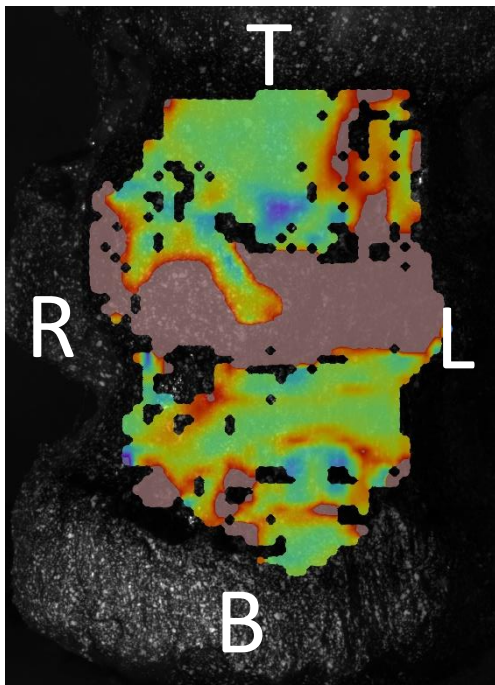


Figure 24 - Maximum eps (ϵ_1) for vertebrae T10 (the uppermost) and T11 (the lowermost) (#775), under a load of 0.75BW.

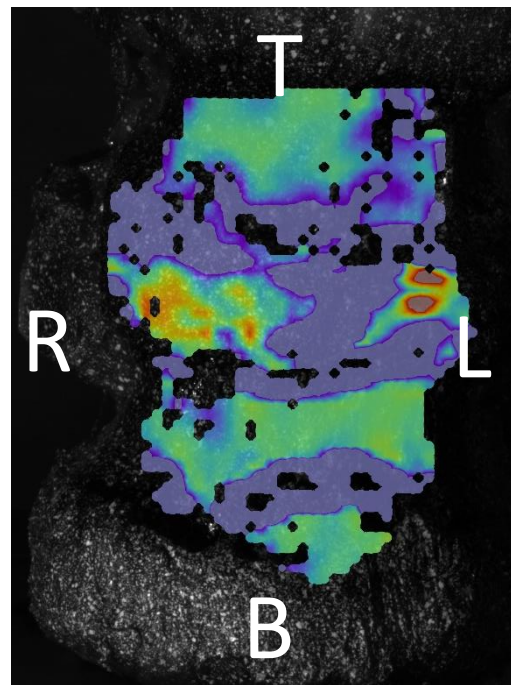


Figure 25 - Minimum eps (ϵ_2) for vertebrae T10 (the uppermost) and T11 (the lowermost) (#775), under a load of 0.75BW.

Vertebra: L2
Specimen: 775

Figure 26 - Masks for vertebra L2 (#775). Lytic lesions were found in the central section, posteriorly, on the right side.

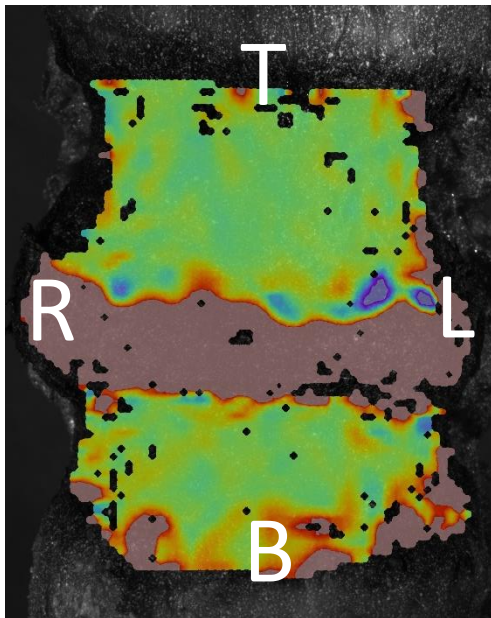
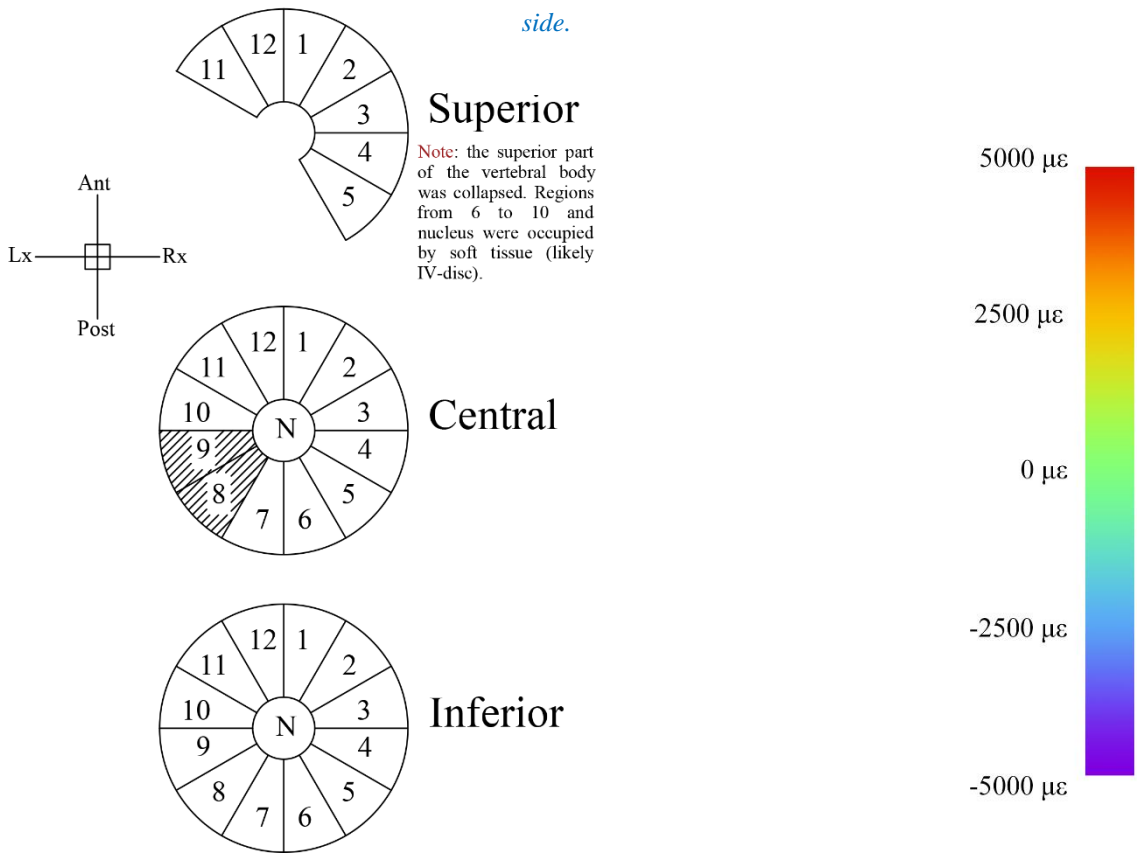


Figure 27 - Maximum ϵ_1 for vertebrae L1 (the uppermost) and L2 (the lowermost) (#775), under a load of 1.5BW.

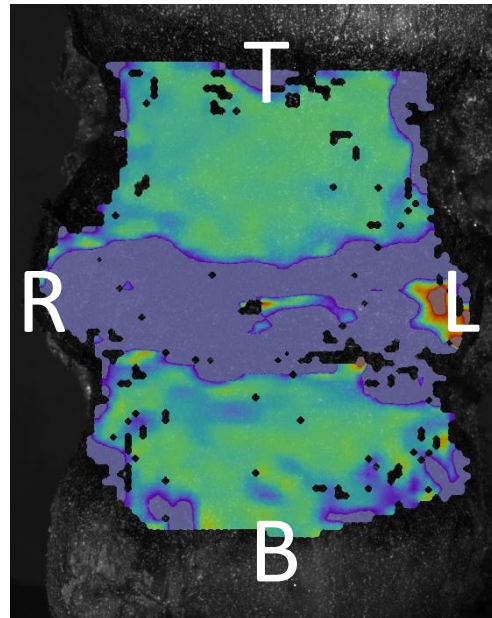


Figure 28 - Maximum ϵ_2 for vertebrae L1 (the uppermost) and L2 (the lowermost) (#775), under a load of 1.5BW.

3.1.3 Qualitative and Qualitative Analyses: Specimen 779

Two segments were obtained from the specimen 779.

The first specimen was composed by three complete vertebrae (T3, T4, and T5). Two of these vertebrae (T4 and T5) were metastatically involved with lytic lesions, in one of them (T5) a capsule of cortical bone enclosed the lesion. Vertebra T3 served as a control. In vertebra T4 ([figure 29](#)), the lesion was located anteriorly both in the superior and central part. Centrally, the lesion was widely spread, occupying both the right and left sides (anteriorly) and the nucleus.

In vertebra T5 ([figure 30](#)), the lesion was located anteriorly in the inferior section.

Being the control available, the strain mean value was normalized for both T4 and T5.

For T4, the normalized mean value for the maximum eps was 0.80 (0.5BW), and 6.4 (1BW). For the minimum eps, the normalized mean value was -14.29 (0.5BW), and 1.95 (1BW).

For T5, maximum eps had a normalized mean value of 0.13 (0.5BW), and 2.1 (1BW).

The normalized mean value for minimum eps was -0.29 (0.5BW), and 0 (1BW).

From a qualitative point of view, high strain fields were found on the superior and central sections of T4, both for minimum and maximum eps. In the central section, these high strains were found in the vicinity of the metastatic regions. In the superior sections, the strains widely spread on the surface, even on non-metastatic regions. Inferiorly, both zones with high and low strains were found, even if evidence of metastases were not found by the use of the masks.

On T5, peaks in eps1 were found at the right and left sides of the metastatic region.

The second segment obtained from specimen 779 was composed of two complete vertebrae (T8 and T9). Of these, we studied T8, while T9 served as a control.

Mixed lesions were found in T8. Lytic lesions were found both in the superior and central sections, on the left side of the specimen ([figure 33](#)).

The normalized mean value for maximum eps was found to be 0.52 (0.5BW), 0.53 (1BW), and 7.45 (1.5BW). For minimum eps, the normalized mean value was 1.16 (0.5BW), 1.37 (1BW), and 2.26 (1.5BW).

Strains of slightly greater magnitude than the rest of the surface were observed near the metastatic regions of T8.

Anomalous peaks were found on the control vertebra (although no evidence of lesions or damages were found on the CT scan).

Specimen 779 - Segment T2^{1/2}-T6^{1/2}

Engineering Principal Strain 1						
Load	0.5 BW			1 BW		
Vertebra	T3	T4	T5	T3	T4	T5
Mean (\pm SD) [$\mu\epsilon$]	7840 (\pm 150)	6300 (\pm 300)	1000 (\pm 200)	1000 (\pm 200)	6400 (\pm 200)	2100 (\pm 100)
Minimum [$\mu\epsilon$]	-11126	-37131	-2550	-1907	-20569	-2451
Maximum [$\mu\epsilon$]	183050	157529	9076	14876	94117	19521

Engineering Principal Strain 2						
Load	0.5 BW			1 BW		
Vertebra	T3	T4	T5	T3	T4	T5
Mean (\pm SD) [$\mu\epsilon$]	700 (\pm 200)	-10000 (\pm 200)	-200 (\pm 200)	-410 (\pm 110)	-800 (\pm 200)	0 (\pm 190)
Minimum [$\mu\epsilon$]	-169714	-254687	-13113	-13828	-189435	-16455
Maximum [$\mu\epsilon$]	51375	19137	1857	1317	9888	3012

Table 7 - The table shows the mean value, the maximum, and the minimum eps (both 1 and 2) for vertebrae T3, T4, and T5 (specimen 779) in the ROI.

Specimen 779 - Segment T7^{1/2}-T10^{1/2}

Engineering Principal Strain 1						
Load	0.5 BW		1 BW		1.5 BW	
Vertebra	T8	T9	T8	T9	T8	T9
Mean (\pm SD) [$\mu\epsilon$]	310 (\pm 150)	600 (\pm 130)	830 (\pm 160)	1570 (\pm 160)	940 (\pm 180)	7000 (\pm 200)
Minimum [$\mu\epsilon$]	-827	-667	-1516	-333	-2652	-3400
Maximum [$\mu\epsilon$]	2309	7675	8895	14861	13255	9500

Engineering Principal Strain 2						
Load	0.5 BW		1 BW		1.5 BW	
Vertebra	T8	T9	T8	T9	T8	T9
Mean (\pm SD) [$\mu\epsilon$]	-800 (\pm 120)	-690 (\pm 70)	-1450 (\pm 130)	-1060 (\pm 80)	-1920 (\pm 160)	-850 (\pm 110)
Minimum [$\mu\epsilon$]	-8171	-3280	-5973	-3214	-13600	-9541
Maximum [$\mu\epsilon$]	447	569	124	162	441	2100

Table 8 - The table shows the mean value, the maximum, and the minimum eps (both 1 and 2) for vertebrae T8 and T9 (specimen 779) in the ROI.

Vertebra: T4
Specimen: 779

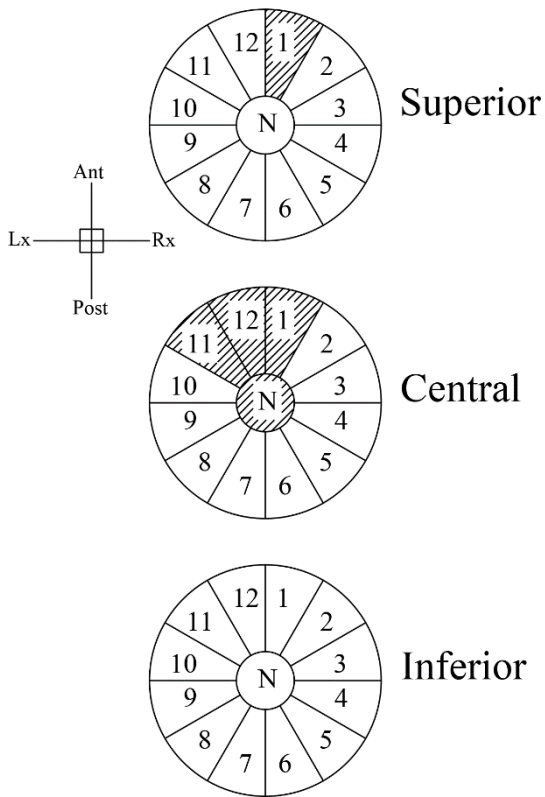


Figure 29 - Masks for vertebra T4 (#779).

Vertebra: T5
Specimen: 779

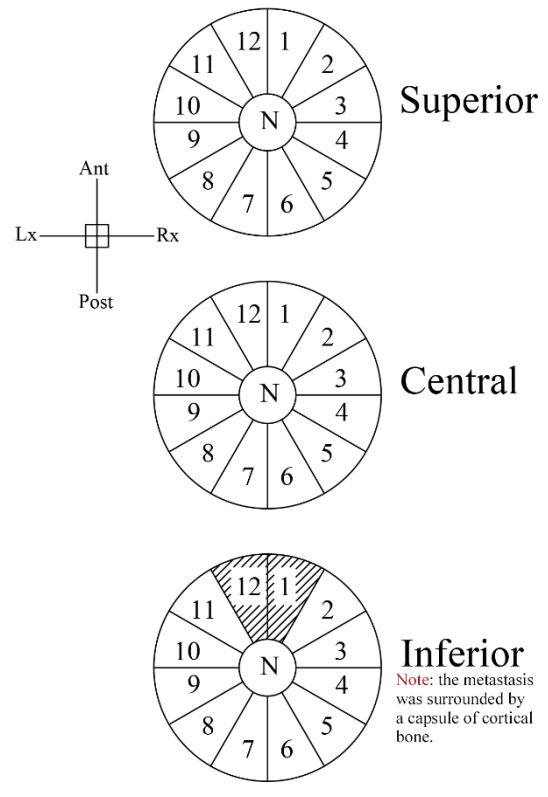


Figure 30 - Masks for vertebra T5 (#779).

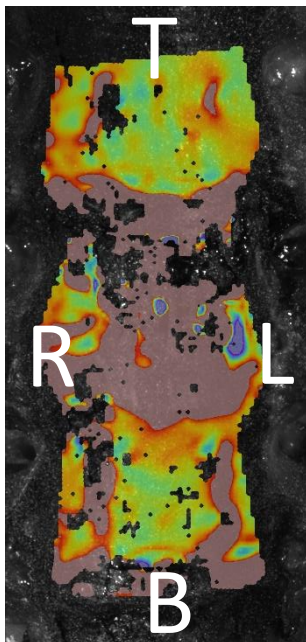


Figure 31 - Maximum ϵ_1 for the segment $T2\frac{1}{2}$ - $T6\frac{1}{2}$ (#779), under a load of 1BW.

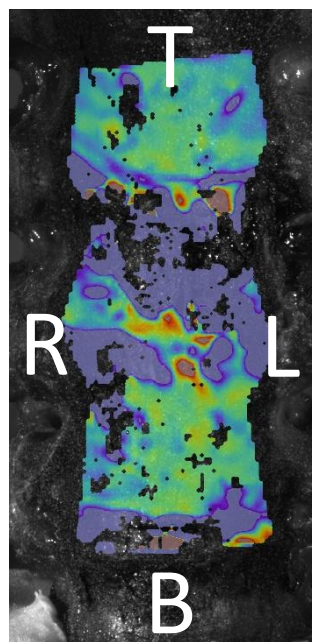


Figure 32 - Minimum ϵ_2 for the segment $T2\frac{1}{2}$ - $T6\frac{1}{2}$ (#779), under a load of 1BW.



Vertebra: T8
Specimen: 779

Figure 33 - Masks for vertebra T8 (#779). Mixed lesions were found within the vertebral body. Lytic lesions were located laterally in the superior and central sections.

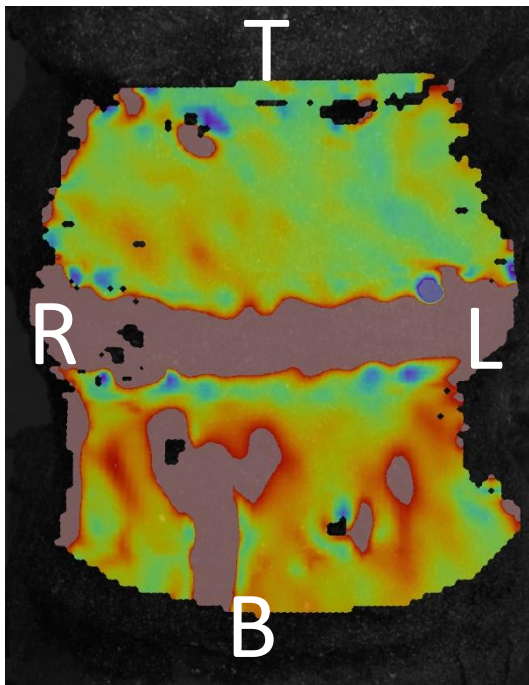
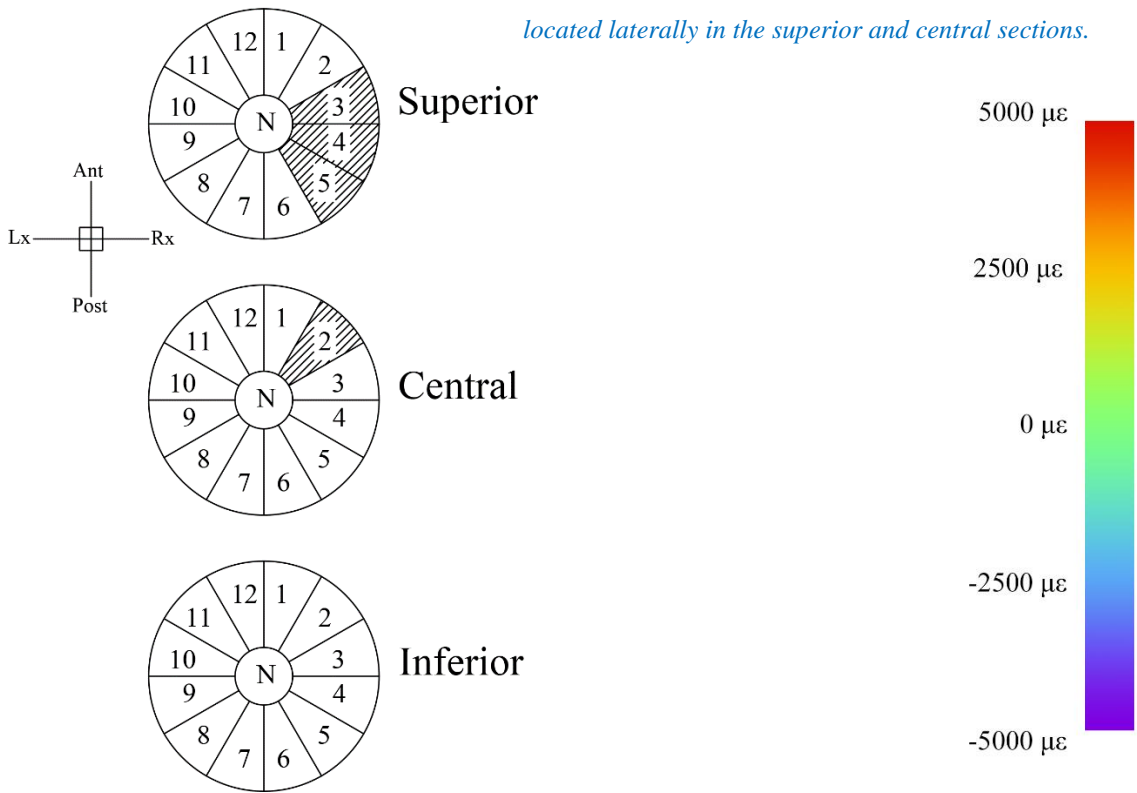


Figure 34 - Maximum eps (ϵ_1) for the segment T7½-T10½ (#779), under a load of 1.5BW. The uppermost vertebra is T8.

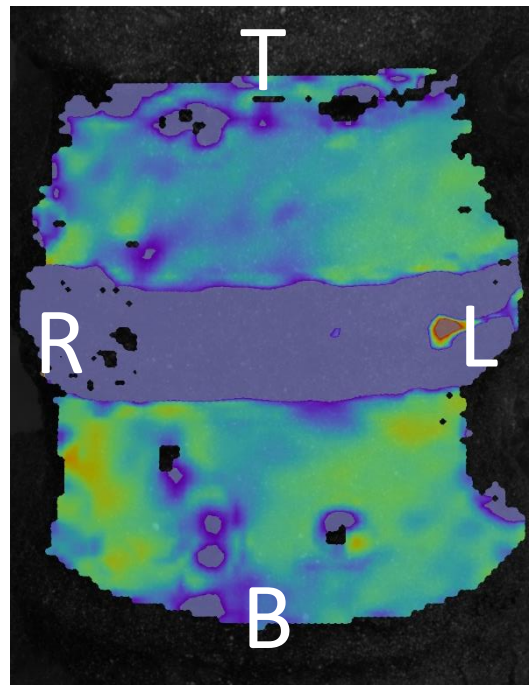


Figure 35 - Minimum eps (ϵ_2) for the segment T7½-T10½ (#779), under a load of 1.5BW. The uppermost vertebra is T8.

3.1.4 Qualitative and Qualitative Analyses: Specimen 784

A two vertebrae (T7 and T8) segment was obtained from the specimen 784.

Of these two vertebrae, T8 was involved with mixed metastases. Lytic lesions were located both anteriorly (in the central and inferior sections) and posteriorly (in the superior section) (figure 36).

Normalized mean strain value were computed for vertebra T8. Normalized mean values for maximum eps were -0.09 (0.5BW) and -0.2 (1BW). For minimum eps, normalized mean values were 0.22 (0.5BW) and 0.78 (1BW).

Qualitative analysis didn't show any correlation between the metastases' location and the strains. On the contrary, high strains (both maximum and minimum) were found on the surface of the control vertebra.

Specimen 784 - Segment T6^{1/2}- T9^{1/2}

Engineering Principal Strain 1				
Load	0.5 BW		1 BW	
Vertebra	T7	T8	T7	T8
Mean (\pm SD) [$\mu\epsilon$]	110 (\pm 100)	-10 (\pm 120)	50 (\pm 120)	-10 (\pm 150)
Minimum [$\mu\epsilon$]	-1924	-651	-370	-431
Maximum [$\mu\epsilon$]	9249	1237	2050	1051

Engineering Principal Strain 2				
Load	0.5 BW		1 BW	
Vertebra	T7	T8	T7	T8
Mean (\pm SD) [$\mu\epsilon$]	-1080 (\pm 70)	-240 (\pm 120)	-460 (\pm 80)	-360 (\pm 140)
Minimum [$\mu\epsilon$]	-16819	-3426	-4417	-2866
Maximum [$\mu\epsilon$]	826	248	-177	287

Table 9 - The table shows the mean value, the maximum, and the minimum eps (both 1 and 2) for vertebrae T7 and T8 (specimen 784) in the ROI.

Vertebra: T8
Specimen: 784

Figure 36 - Masks for vertebra T8 (#784). The vertebra was involved with mixed lesions. Lytic lesions were found laterally in the inferior, central, and superior sections.

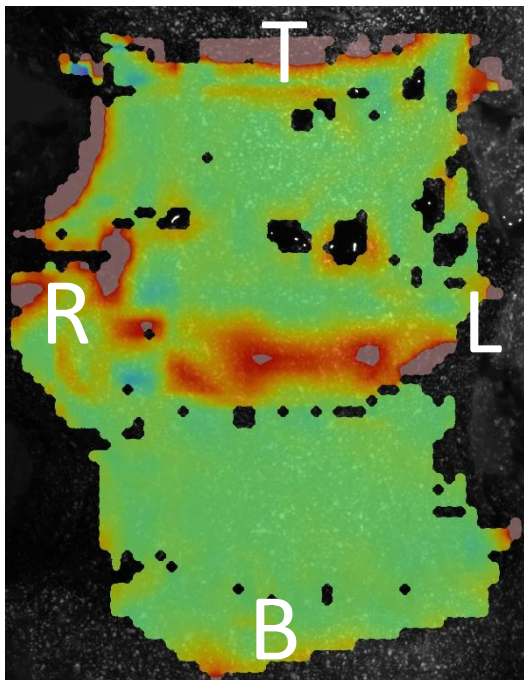
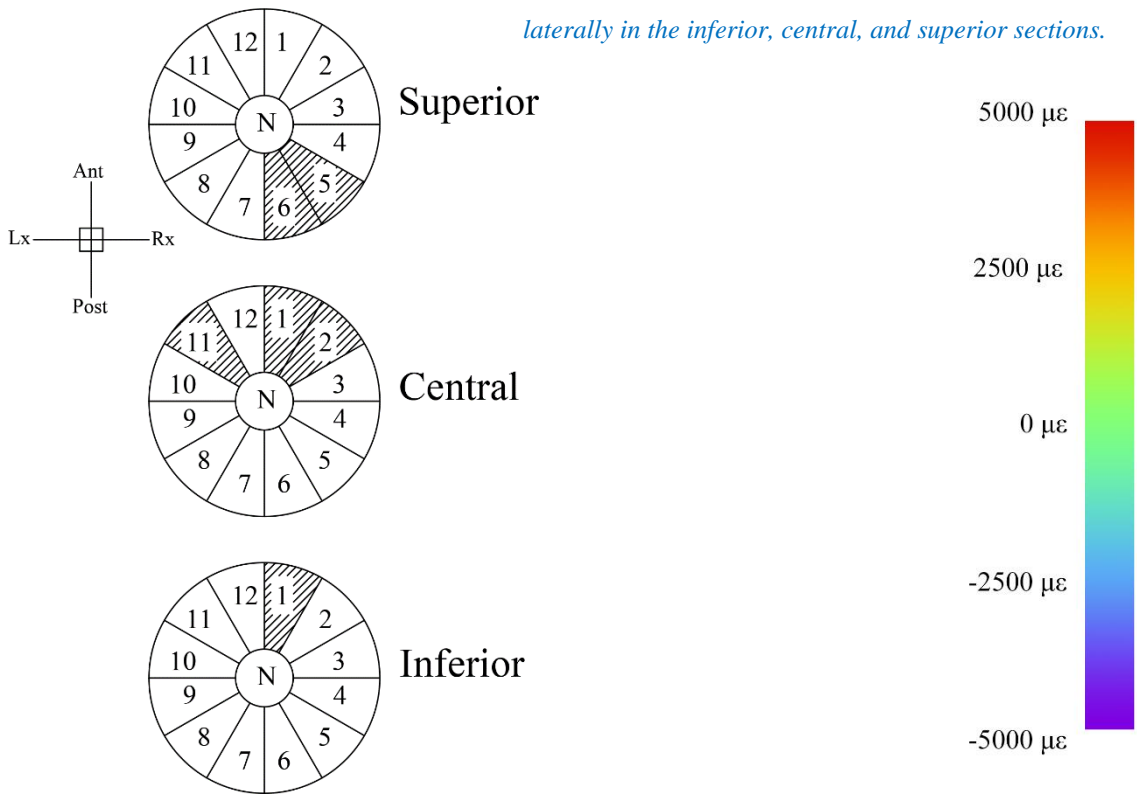


Figure 37 - Maximum eps (ϵ_1) for the segment T6½-T9½ (#784), under a load of 1BW. The uppermost vertebra is T7.

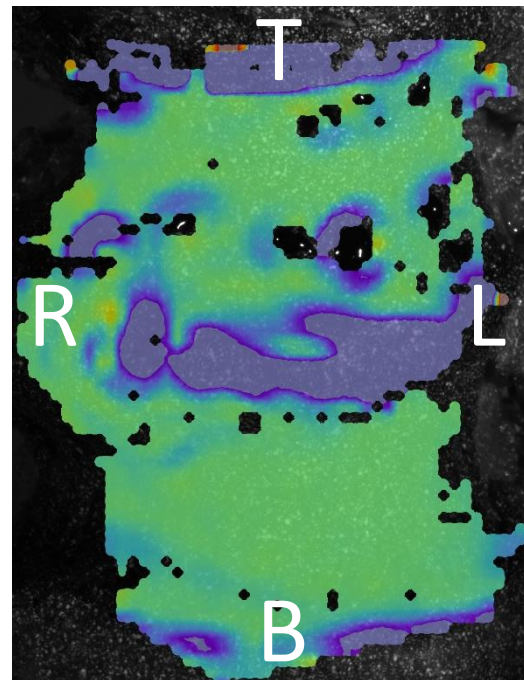


Figure 38 - Minimum eps (ϵ_2) for the segment T6½-T9½ (#784), under a load of 1BW. The uppermost vertebra is T7.

3.1.5 Qualitative and Qualitative Analyses: Specimen 785

A segment of three complete vertebrae (T5, T6, and T7) was obtained from specimen 785.

Two of the three vertebrae (T5 and T6) were metastatically involved with lytic metastases. T7 was used as control.

On T5 (figure 39), metastases were located posteriorly on the right side (both in the inferior and central sections). In T6 (figure 40), lytic lesions were found in the superior and central sections, posteriorly.

For T5, the normalized mean value of maximum eps was 7.57 (0.5BW), 1.67 (1BW), and 4.6 (1.5BW). The normalized mean value for minimum eps was 2.63 (0.5BW), 0 (1BW), and -0.22 (1.5BW).

For T4, the normalized mean value found for maximum eps was 4.29 (0.5BW), 1.33 (1BW), and 0.4 (1.5BW). The normalized mean value for minimum eps was 2.39 (0.5BW), 1 (1BW), and 0.89 (1.5BW).

Low correlation between the location of lesions and the field of strain was found. Significant strains were seen on vertebra T6 all over the surface, both when maximum and minimum eps were showed. Significant strains were found also on vertebra T5, near the location of metastases (but also in the vicinity of intervertebral disc, which could as well be the cause).

Specimen 785 - Segment T4½-T8½

Engineering Principal Strain 1						
Load	0.5 BW			1 BW		
Vertebra	T5	T6	T7	T5	T6	T7
Mean (\pm SD) [$\mu\epsilon$]	530 (\pm 190)	300 (\pm 200)	70 (\pm 180)	500 (\pm 200)	400 (\pm 300)	300 (\pm 300)
Minimum [$\mu\epsilon$]	-149	-13	-81	-66	6	-398
Maximum [$\mu\epsilon$]	11037	2628	715	1359	2116	5681

Engineering Principal Strain 2						
Load	0.5 BW			1 BW		
Vertebra	T5	T6	T7	T5	T6	T7
Mean (\pm SD) [$\mu\epsilon$]	-1210 (\pm 150)	-11000 (\pm 200)	-460 (\pm 130)	0 (\pm 200)	-600 (\pm 200)	-600 (\pm 200)
Minimum [$\mu\epsilon$]	-12848	-8119	-2522	-835	-1883	-3968
Maximum [$\mu\epsilon$]	258	6	-41	399	181	174

Table 10 - The table shows the mean value, the maximum, and the minimum eps (both 1 and 2) for vertebrae T5, T6, and T7 (specimen 785) in the ROI.

Specimen 785 - Segment T4½-T8½ (bis)

Engineering Principal Strain 1			
Load	1.5 BW		
Vertebra	T5	T6	T7
Mean (\pm SD) [$\mu\epsilon$]	2300 (\pm 300)	200 (\pm 300)	500 (\pm 300)
Minimum [$\mu\epsilon$]	-398	-627	131
Maximum [$\mu\epsilon$]	5681	26706	1440

Engineering Principal Strain 2			
Load	1.5 BW		
Vertebra	T5	T6	T7
Mean (\pm SD) [$\mu\epsilon$]	200 (\pm 300)	-800 (\pm 200)	-900 (\pm 200)
Minimum [$\mu\epsilon$]	-14783	-1842	-2293
Maximum [$\mu\epsilon$]	1395	72	338

Table 10 (bis) - Mean value, maximum, and minimum eps (both 1 and 2) for vertebrae T5, T6, and T7 (specimen 785) under a load of 1.5BW.

Vertebra: T5
Specimen: 785

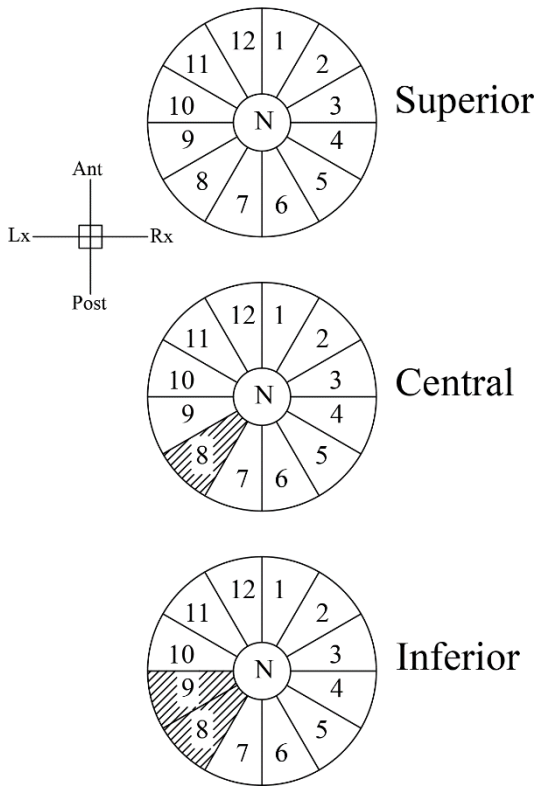


Figure 39 - Masks for vertebra T5 (#779).

Vertebra: T6
Specimen: 785

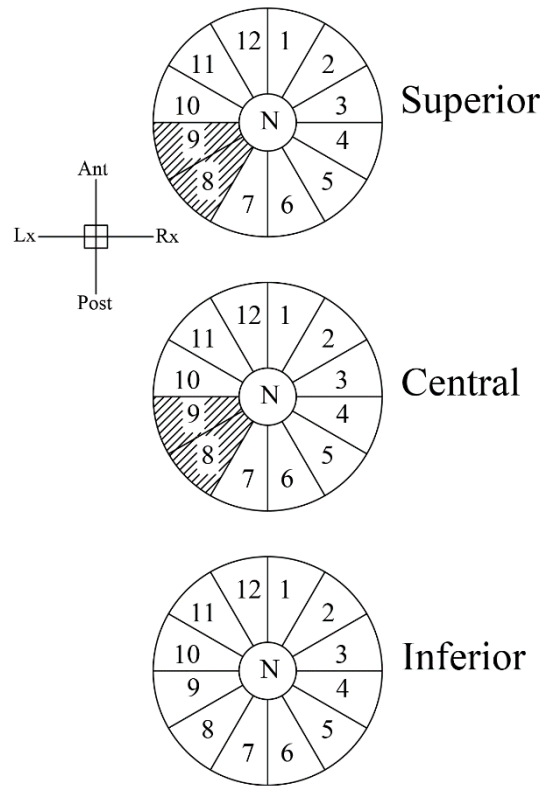


Figure 40 - Masks for vertebra T6 (#779).

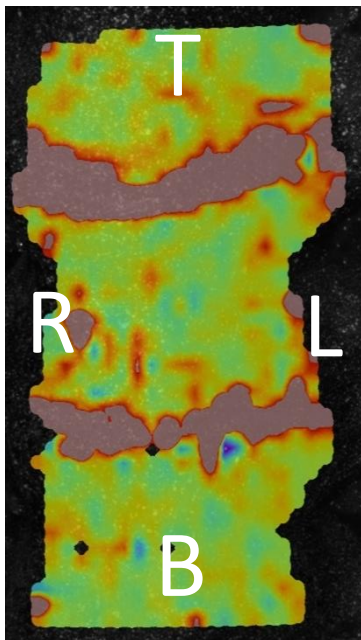


Figure 41 - Maximum ϵ_1 for the segment $T4\frac{1}{2}$ - $T8\frac{1}{2}$ (#785), under a load of 1.5BW. The cranial end is the top of the figure.

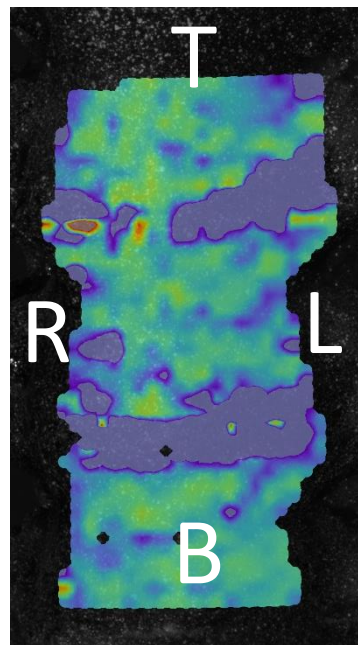
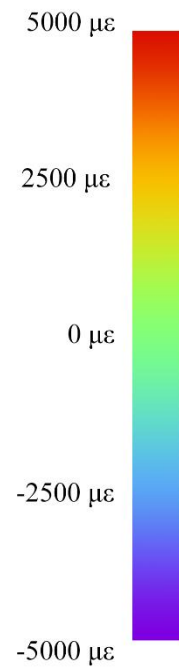


Figure 42 - Minimum ϵ_2 for the segment $T4\frac{1}{2}$ - $T8\frac{1}{2}$ (#785), under a load of 1.5BW. The cranial end is the top of the figure.



3.1.6 Qualitative and Qualitative Analyses: Metastases Size

An approximation of the lytic metastases volume was computed for each of the metastatic vertebrae analyzed. An approximate volume was obtained also for the vertebra itself and employed to normalize the dimensions of the lesion.

Table 10 shows the approximated volumes of vertebrae and metastases, as well as the normalized volume of each metastasis.

Vertebra					Lesion		
Specimen	Position	CC Size (mm)	RL Size (mm)	Volume (mm ³)	Diameter (mm)	Volume (mm ³)	Normalized Volume (%)
775	T11	22	301	16605	8	268	1.6
					8	268	1.6
					7	180	1.1
	L2	19	39	22697	7	180	0.8
779	T4	14	26	7433	10	524	7.0
	T5	19	23	7894	5	65	0.8
	T8	14	30	9896	12	905	9.1
784	T8	20	27	11451	5	65	0.6
					11	697	6.1
785	T5	15	23	6232	8	268	4.3
	T6	16	20	5027	10	524	10.4

Table 12 - The table shows the approximated volume of vertebrae and lesions. The vertebrae were considered as cylinders, with CC size as height and RL size as diameter. Lesions were modeled as spheres whose diameter was the maximum width on the transversal plane of the VB.

3.2 Repeatability Tests

3.2.1 Repeatability Tests: Results of Test for Intra-Operator Repeatability

Intra-operator repeatability was tested through the repetition of the whole process of sample acquisition and mask creation, and by repetition of the lesions' identification phase only on a selected number of frames.

Regarding the repetition of the entire process, the top sample was observed to be the least repeatable (up to three regions resulted in a different evaluation), the bottom sample was observed to be the most repeatable (in only one out of three vertebrae, a region received a different evaluation). In terms of repeatability, the central sample was positioned between these two.

The low repeatability of the top and central samples could be explained as a combined effect of approximation and sampling process (samples were obtained proceeding from the caudal to the cranial end). In addition, slight differences in the starting point could have influenced the resulting sample. In the end, it resulted in larger whereabouts for the measurements steps.

The evaluation was found to be more repeatable when only the last steps (i.e. mask creation and lesion identification) were repeated. The identification of lesions in tissue characterized by a high contrast (i.e. when both light and dark shades of gray were present) resulted to be the least repeatable (in one case, two regions received a different evaluation from the other two repetitions).

3.2.2 Repeatability Tests: Results of Test for Inter-Operator Repeatability

Inter-operator repeatability was tested on nine samples (with pre-built masks) from three vertebrae. The four operators were tasked with localizing the metastases within the masks. Location was found to be highly repeatable for samples with mixed metastases. This was probably due to the high contrast between newly developed metastatic bone and osteolytic lesions.

The samples with sparsely distributed low-density tissue (which was assumed as an effect of osteoporosis) were found to be the least repeatable. In one case, two operators assessed

the sample as healthy, while the other two found respectively two and five metastatic regions.

Chapter 4: Discussion

Eight segments with one or two metastatic vertebrae were tested in presso-flexion. By mean of DIC, we obtained a 3D reconstruction of the field of strain distribution for each of the tested segments.

The field of strain was analyzed both qualitatively and quantitatively. Our main aim was to assess the influence of lytic lesions' size and location on the resulting strain of field.

In general, we observed that:

- The strain fields of healthy vertebrae were homogeneous. When the loading conditions (i.e. magnitude of the load imposed) changed, the superficial strains' mean value experienced a variation above the 30% *circa*;
- Far from being homogeneous, the strain fields of vertebrae with lytic metastases showed significant strain peaks. Inside the metastatic vertebra, the overhaul variation of the superficial strains' mean value was under 30% *circa*;
- In vertebrae involved with blastic metastases, the field of strain resulted to be homogeneous with low strain values;
- The field of strain in vertebrae with mixed metastases showed features often similar to vertebrae with blastic lesions.

Regarding the influence of metastases location, we found that lesions located anteriorly (i.e. lesions within the regions from 10 to 3) were often associated with peaks on the field of strain distribution (both for eps1 and eps2), regardless of their size. Assuming the action of the osteoclasts to be random, we could hypothesize that these peaks were caused by an interruption of the trabecular pattern and the subsequent formation of a "stress concentrator". This would lead to a new question, is there a minimum size for which the metastasis' action cannot be consider equal to a stress concentrator?

We found some exceptions to the previous findings, the most notable being linked with the presence of blastic lesions (vertebra T8 in specimen 784) and the presence of capsules of cortical bone around the lytic metastases (vertebra T5 in specimen 779).

Regarding metastases with capsule, peaks on the strain field distribution were observed in the area surrounding the metastasis but not on the metastasis itself. It could be that a

discontinuity in the density of the bony tissue might cause a redistribution of the loads. The trabecular bone surrounding the capsule would receive the larger part of the load (thus explaining the significant strains), meanwhile, the sturdy cortical bone of the capsule would experience a zero-strain condition.

Lesions located posteriorly (i.e. within the regions from 4 to 9) did not influence significantly the field of strain distribution, even if their size was significant (e.g. 10.4% of the vertebral body for T6, specimen 785). This was likely due to the posterior arc sharing part of the load. However, this is but a hypothesis, lateral acquisition should be performed to verify its correctness.

We were not able to determine whether lesions within the nucleus could cause significant peaks of strain. The nucleus was involved only in one case out of eight, and, even in that case, the peaks on the strain field were likely due to the lesions on surface of the vertebral body.

In vertebrae involved with mixed lesions, the field of strain was not influenced by either the location or the dimension of the lytic lesions.

In general, the behavior of vertebrae with mixed and blastic-only lesions could be confounded. In both cases, the field of strain resulted to be rather homogeneous, with peaks only in the vicinity of the intervertebral disc.

The size of the metastases did not seem to have a significant influence over the superficial strains. As previously stated, regardless of the size, lesions located anteriorly in vertebrae with lytic-only metastases seemed to be the cause of significant peaks in the strain field. On the other hand, if a large metastasis was located posteriorly within the vertebral body, it would not have caused alteration to the field of strain distribution.

The results partly contrasted with the studies currently published regarding the mechanical behavior of metastatically involved vertebrae.

Location was found to hold an important role in determining the field of strain distribution. However, unlike Tschirhart's findings (Tschirhart, Nagpurkar, & Whyne, 2004), anteriorly located lesions were found to cause a major vertebral bulge, while the impact of posteriorly located lesions was negligible.

Contrary to Whyne's study (Whyne, Hu, & Lotz, 2001), the impact of the size was found to have a small relevance on the strain field distribution.

Compared to previous DIC-based studies (Palanca, Barbanti-Bròdano, & Cristofolini, 2018), this work highlighted that the influence of real metastasis on the field of strain distribution can be significant even when the lesion's size is reduced.

The discrepancy between our findings and the previous was probably due to the work's nature. Contrary to a large part of the literature, we tested vertebrae with actual metastases, which might differ significantly from vertebrae with simulated lesions, both under the point of view of mechanical behavior and morphology. The coexistence of blastic and lytic lesions in the studied vertebrae should be considered as a possible cause of this divergency. Lastly, the estimated size of actual lytic lesions was found to be significantly smaller than simulated lesions'; in particular, the size simulated lesions in the literature ranged from 10% to 50 % of the vertebral body, while the maximum size of lytic lesions in this study was 10% of the vertebral body.

The limitations of the study at the current might make it difficult to draw clear conclusions.

First of all, the masks were built on three samples which were assumed to represent an entire section of the vertebra (equal to a third of its height). This process of "discretization" was associated with a significant loss of information (what fell between two samples was lost and, thus, not considered in the analysis of the vertebra).

Secondly, we represented only the most significant lesions, although the results of this study proved that lesions of smaller size can alter the field of strain if located anteriorly on the surface. Furthermore, the studied lesions were all similar size (in 6 case out of 11 they involved less than the 2% of the vertebral body; only a single lesion exceeded a 10% involvement of the vertebra).

The dimension of metastasis was likely underestimated. In fact, we measured the lesions only on the transverse plane of the vertebral body, neglecting to perform measurement on the sagittal and frontal planes. The normalization of the estimated volume had likely caused an additional underestimation (the modelled vertebra likely overfitted the real one).

Regarding the test, we tested the vertebrae under simplified loading condition. The load was assumed to be of pure compression, far from the physiological loading condition (involving a combination of compression, torsion, bending, and shear).

Lastly, with DIC we acquired only the anterior surface of the vertebral body. Lateral acquisition should be performed to assess whether posteriorly located lesions can alter the field of strain distribution.

While one could argue that the number of specimens was insufficient for statistical relevance, this study was meant as a preliminary investigation in support of future works, thus the numerosity was not our primary concern.

Nevertheless, the designed tool (i.e. the mask) proved to be both useful and versatile for this preliminary study; meanwhile, we also obtained valuable results.

Further studies should focus on the improvement of the localization process and on obtaining a more accurate estimate of the volume for both vertebra and the lesion.

Extending the analysis of the strain distribution to the entire surface (and volume) of the vertebra should also be an aim for future studies.

Chapter 5: Conclusions

The literature about the influence of metastasis type, location, and size is scarce and often not exhaustive.

However, before in-depth studies could take place, a preliminary study should be performed to better understand whether or not this direction for research in spine biomechanics might prove fruitful.

With this study we wanted to make this preliminary step.

Our aim was to assess the influence of metastases size and location on the superficial field of strain distribution.

After analyzing eight segments from five spine with metastases, we found that the strain field greatly depends on the metastases type in the first place. In particular, the presence of blastic metastases (whether in vertebrae with mixed or blastic-only lesions) was often associated with homogeneous field of strain, where strains often had low magnitude (in the order of the hundred micro-strain).

Location was found to influence the field of strain distribution in vertebrae solely involved with lytic metastases. Anteriorly located lesions caused significant peaks in the strain field, while posteriorly located lesions did not seem to affect it.

Contrary to previous studies, we found that size was not significantly involved in the alteration of the field of strain distribution. Regardless of their size, small anteriorly located lesions did cause strain peaks, while large posteriorly located lesions did not.

Our findings partly disagreed with the literature available. This was partly due the nature of this work. To the author knowledge this was one of the first works to use specimen with actual metastatic lesions, whereas previous studies focused on specimen with simulated lytic defects.

This preliminary *in vitro* study proved that location should be taken into account when studying the superficial strain distribution. However, there are other factors (such as the type of the metastases involved) that weight more heavily on the mechanical response and they should not be neglected.

Extra Chapter: Addendum

This chapter is intended a collection of supplementary material.

The followings are information that were excluded from the main body of the thesis. The main reason of their exclusion was the scarce pertinence with the aim.

With that in mind, I think that adding this content might result useful to the understanding of the final work.

Additional Information from the CT-generated DICOM Files

- File Size: 526722 B;
- Format: DICOM;
- Format Version: 3;
- Width: 512p;
- Height: 512p;
- Bit Depth: 16;
- Colour Type: grayscale;
- Modality: CT;
- Manufacturer: TOSHIBA;
- Manufacturer Model: Aquilion ONE;
- Scan Options: Helical CT;
- Slice Thickness: 1mm;
- Kilovoltage Peak: 120kV;
- Data Collection Diameter: 320mm;
- Reconstruction Diameter: 128.75mm;
- Exposure Time: 1000 msec;
- X-Ray Tube Current: 200mA;
- Exposure: 200mAs;
- Generator Power: 24kW;
- Spiral Pitch Factor: 0.638;
- Pixel Spacing: 0.251 mm (row), 0.251 mm (column).

Loading Criteria

As reported in Chapter 2 (Section 3.3), the specimens were tested in a condition far from the physiological range.

However, in order to preserve the specimens' integrity, we decided to use progressive loads. We used the loads involved in everyday activities as a reference.

Since the aim of the thesis was neither the simulation of motor tasks nor the study of the response to physiological condition, I have left the choice loading steps unjustified.

In this addendum, I will briefly go over this choice by adding examples of activities which can be related to the loadings used (see [table A1](#)).

The information about the loadings were obtained by consultation of OrthoLoad's database (Charité – Universitätsmedizin Berlin, 2019) for vertebral body replacements.

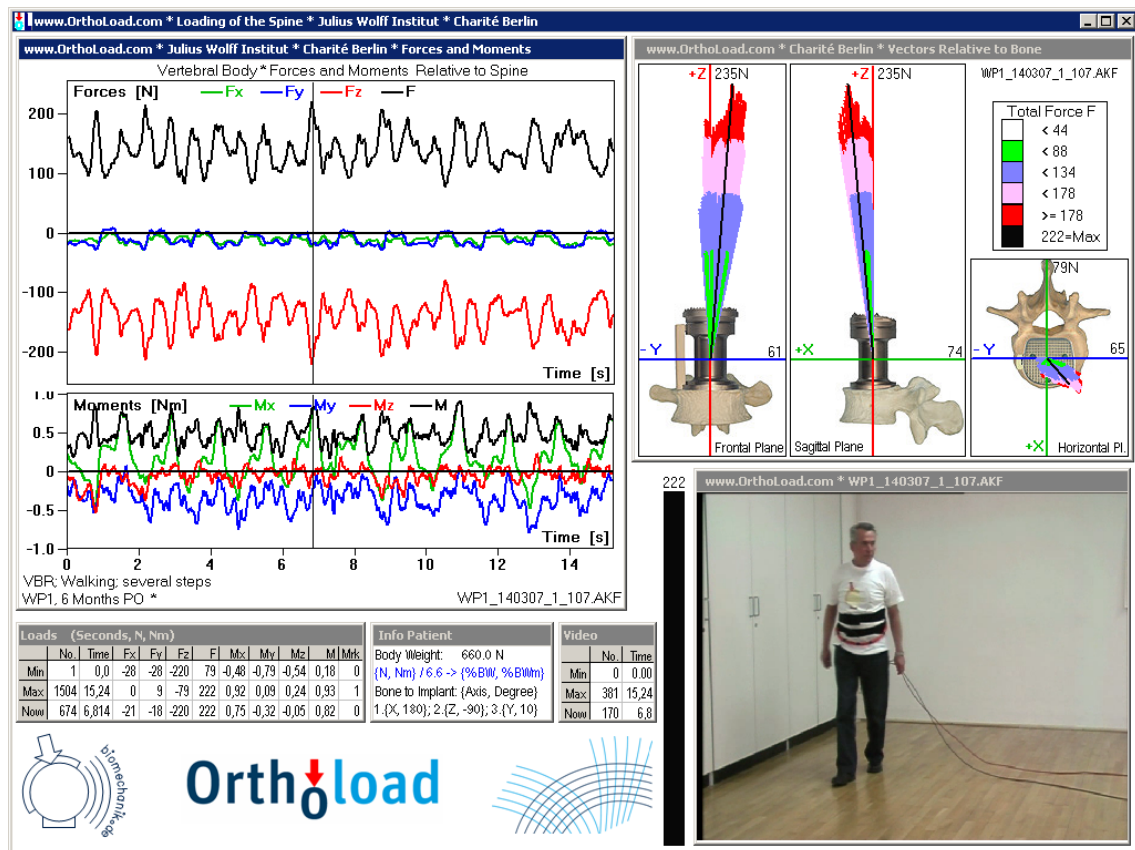


Figure A1 - Queries were submitted to Orthoload's database to obtain a qualitative definition of the loads involved in simple motor tasks.

Research Field						Data		
Implant	Activity	Parameter	Patient	Months PO	File	BW (N)	Max Compression (N)	Max Compression (BW)
VBR	Walking: several steps	None	wp1	6	wp1_140307_1_107	660	222	0.34
				7	wp1_250407_1_70	660	215	0.33
				11	wp1_150807_1_83	660	204	0.31
				12	wp1_050907_1_132	660	215	0.33
				29	wp1_110209_2_47	660	320	0.48
				29	wp1_110209_2_49	660	300	0.45
				44	wp1_290510_3_18	660	400	0.61
				51	wp1_101210_1_152	660	472	0.72
				63	wp1_101210_1_161	660	435	0.66

Compression Mean Value (BW) = 0.47

Compression Standard Deviation (BW) = 0.16

Research Field						Data		
Implant	Activity	Parameter	Patient	Months PO	File	BW (N)	Max Compression (N)	Max Compression (BW)
VBR	Standing: picking something up	None	wp5	18*	wp5_220110_1_83	630	482	0.77
				18	wp5_220110_1_88	630	741	1.18
				24	wp4_200110_1_94	630	717	1.14

*with aid

Compression Mean Value (BW) = 1.03

Compression Standard Deviation (BW) = 0.23

Research Field						Data		
Implant	Activity	Parameter	Patient	Months PO	File	BW (N)	Max Compression (N)	Max Compression (BW)
VBR	Special Activities of Daily Living: tying shoes	None	wp4	24	wp4_200110_1_3	630	698	1.11
				24	wp4_200110_1_61	630	1095	1.74
				24	wp4_200110_1_62	630	836	1.33
				24*	wp4_200110_1_63	630	969	1.54

*with aid

Compression Mean Value (BW) = 1.43

Compression Standard Deviation (BW) = 0.27

Table A1 - The table shows the research parameters used to query OrthoLoad's database and the obtained data. In addition, below each table, the mean value and the standard deviation for compression.

Designing the Process of Mask Creation

This brief paragraph was made to add information about how the mask creation process was designed.

As stated in Chapter 2 (Section 4.1), the idea was to super-impose a custom build mask to a view of the vertebra on the transverse plane.

However, I did not have at my disposal adequate tools (and to date, I do not know if such tools exist).

In its first instance, a “frame” consisted in a view of the vertebra, obtained by means of an in-built tool of synedra View Personal which allows to convert a view to either a .dcm or a .jpg file. However, this tool was soon found to be inadequate for the following reasons:

- RGB conversion: many medical images are grayscale, which means that each pixel can assume one of 2^{16} grays shades; although it is true that not all of the 16 bit (retaining the color information) are used (in general medical images use only 12 of the 16 bit), RGB conversion causes a significant loss of information (assuming that an RGB format uses 8 bit for the luminance, converting a file from GS to RGB means losing 3840 gray shades, if “only” 12 bits were used by the original file);
- Lossy format: .jpg (compatible with CAD software) is lossy compression; to reduce the file size, lossy algorithm discard part of the information retained in the “raw” file.

To reduce the loss of information, I decided to acquire the “frames” in a different way. The second version of the frame acquisition step involved the use of Photoshop (Adobe, San Jose, CA, US). Photoshop allowed to convert the DICOM files to grayscale .png (which is a lossless file format) files.

However, new problems rose:

- .png conversion could be performed only on single slices (and the slices of a CT-scan, in general, are not view of the transverse plane of the vertebra);
- Being constrained by the use of single slices, I could not obtain the frames at the desired height (that is 1/6, 1/2, and 5/6 of the cranio-caudal size).

The final version (that is the one adopted in the thesis) was designed to solve these problems and find a balance between the two previous methods.

Following the advice of Marco Palanca, the solution that I have adopted made use of screenshot of the vertebra (viewed in multiplanar reconstruction through the viewer).

The screenshots had an adequate resolution (1920×1080 pixels) and were saved in a lossless format (.png).

Acquiring screenshots implied a loss of information in terms of shades of gray (colors were represented in RGB not GS); however, this loss of information was considered an acceptable price to pay for the greater versatility.

Details Regarding Inter-/Intra- Operator Tests

I wanted to include a detailed exposition of the intra- and inter- operator test. However, a detailed analysis of the tests for the “tool” (i.e. mask) was beyond this work’s aims. By adding this analysis in the addendum, on the other hand, I was able to preserve the work’s coherence and provide a detailed report of the tests altogether.

As previously explained, I decided to lead three tests in total. Two tests were aimed at assessing the intra-operator repeatability, the other one focused on testing inter-operator repeatability.

The material for the test (i.e. the frames) were obtained by three vertebrae. These vertebrae belonged to the same specimen, that is the specimen 779. The reason of this choice lied in the high variety of tissues’ morphology (i.e. healthy, with blastic and lytic lesions, osteoporotic) found in the vertebrae. These vertebrae were also marked by the oncologist as possible cases of study.

The first test to be designed aimed at assessing the repeatability of the whole process of identification. For three days I repeated the same process which involved: (1) measuring the cranio-caudal size of the vertebra, (2) obtaining a “frame” of the vertebrae at the three defined height, (3) building the masks, and (4) identifying the lesions.

Given that the entire process was repeated and, subsequently, the “frames” pertained to a roundabout rather than a same location, the results were quite satisfying.

The second intra-operator test was designed to ascertain whether repeatability could improve by using the same “frames”. In order to do that, I took the “frames” acquired on the first day for the first intra-operator test and their results. For the next two days I repeated the last two steps of the process (i.e. mask creation and lesion identification).

The new evaluations were found to be more repeatable. I also assessed by eye that, in general, a mask built on a certain vertebra matched those built on the same vertebra in different days.

For the inter-operator repeatability test, I decided to use “frames” with prebuild masks. This choice was made mainly for one reason: if the entire process was to be repeated, I would not been able to ascertain whether different evaluations were due to different interpretations or differently looking frames altogether. Nevertheless, I am led to believe

that, if the operators were tasked with building new mask, the results would have not been so dissimilar to those obtained.

The “frames” used were those acquired on day one of the first intra-operator test.

Four candidates for the inter-operator tests were found among the students of biomedical engineering. This choice was mainly made for three reasons: (1) to have a homogeneous population, with a similar educational background; (2) to emulate the final users (the “tool” was not aimed for clinical use but for research); (3) to have candidates with a preparation not unlike mine.

The results were mixed. On the one hand, a general agreement was found over the identification of larger lesions. On the other hand, smaller lesions led to overhaul diverse evaluations. Osteoporotic tissues were also evaluated differently.

For this reason and for the feedback received during the inter-operator tests, I decided to modify the “tool”. In the final version (that is, the version through which the masks in “Results” are obtained), only the larger lesions were located, while smaller lesions were assumed to have a negligible influence. The definition of a “large” and “small” lesions was left to the user discretion.

The results of the various test can be found in the next pages.

INTRA-OPERATOR TESTS (FULL REPETITION) [1 of 3]

		Section												
		1	2	3	4	5	6	7	8	9	10	11	12	N
Day	1												X	
	2												X	
	3												X	

Specimen: 779
Vertebra: T4
Section: Inf

		Section												
		1	2	3	4	5	6	7	8	9	10	11	12	N
Day	1	X	X									X	X	X
	2	X	X									X	X	X
	3	X	X									X	X	X

Specimen: 779
Vertebra: T4
Section: Cen

		Section												
		1	2	3	4	5	6	7	8	9	10	11	12	N
Day	1	X		X							X	X	X	X
	2	X	X	X							X	X	X	X
	3	X	X	X										X

Specimen: 779
Vertebra: T4
Section: Sup

INTRA-OPERATOR TESTS (FULL REPETITION) [2 of 3]

		Section												
		1	2	3	4	5	6	7	8	9	10	11	12	N
Day	1												X	
	2	X											X	
	3	X											X	

Specimen: 779
Vertebra: T5
Section: Inf

		Section												
		1	2	3	4	5	6	7	8	9	10	11	12	N
Day	1													
	2													
	3													

Specimen: 779
Vertebra: T5
Section: Cen

		Section												
		1	2	3	4	5	6	7	8	9	10	11	12	N
Day	1													
	2													
	3													

Specimen: 779
Vertebra: T5
Section: Sup

INTRA-OPERATOR TESTS (FULL REPETITION) [3 of 3]

		Section													
		1	2	3	4	5	6	7	8	9	10	11	12	N	
Day	1														Specimen: 779
	2														Vertebra: T8
	3														Section: Inf

		Section													
		1	2	3	4	5	6	7	8	9	10	11	12	N	
Day	1		X	X	X							X			Specimen: 779
	2		X	X	X	X						X			Vertebra: T8
	3		X	X	X	X						X			Section: Cen

		Section													
		1	2	3	4	5	6	7	8	9	10	11	12	N	
Day	1			X	X	X	X				X	X			Specimen: 779
	2			X	X	X									Vertebra: T8
	3			X	X	X	X					X			Section: Sup

NOTE: The first intra-operator tests took place between September the 13th and September the 15th. Each day, the full process was repeated for each of the three vertebrae.

INTRA-OPERATOR TESTS (PARTIAL REPETITION) [1 of 3]

		Section												
		1	2	3	4	5	6	7	8	9	10	11	12	N
Day	1												X	
	2												X	
	3												X	

Specimen: 779
Vertebra: T4
Section: Inf

		Section												
		1	2	3	4	5	6	7	8	9	10	11	12	N
Day	1	X	X									X	X	X
	2	X	X									X	X	X
	3	X	X									X	X	X

Specimen: 779
Vertebra: T4
Section: Cen

		Section												
		1	2	3	4	5	6	7	8	9	10	11	12	N
Day	1	X		X							X	X	X	X
	2	X	X	X							X	X	X	X
	3	X	X	X							X	X	X	X

Specimen: 779
Vertebra: T4
Section: Sup

INTRA-OPERATOR TESTS (PARTIAL REPETITION) [2 of 3]

		Section												
		1	2	3	4	5	6	7	8	9	10	11	12	N
Day	1												X	
	2												X	
	3												X	

Specimen: 779
Vertebra: T5
Section: Inf

		Section												
		1	2	3	4	5	6	7	8	9	10	11	12	N
Day	1													
	2													
	3													

Specimen: 779
Vertebra: T5
Section: Cen

		Section												
		1	2	3	4	5	6	7	8	9	10	11	12	N
Day	1													
	2													
	3													

Specimen: 779
Vertebra: T5
Section: Sup

INTRA-OPERATOR TESTS (PARTIAL REPETITION) [3 of 3]

		Section													
		1	2	3	4	5	6	7	8	9	10	11	12	N	
Day	1														Specimen: 779
	2														Vertebra: T8
	3														Section: Inf

		Section													
		1	2	3	4	5	6	7	8	9	10	11	12	N	
Day	1		X	X	X							X			Specimen: 779
	2		X	X	X								X		Vertebra: T8
	3		X	X	X							X			Section: Cen

		Section													
		1	2	3	4	5	6	7	8	9	10	11	12	N	
Day	1			X	X	X	X				X	X			Specimen: 779
	2			X	X	X						X			Vertebra: T8
	3			X	X	X						X			Section: Sup

NOTE: The second version of the intra-operator was designed around September the 15th. The tests begun on September the 16th and ended on September the 17th. I used the first of the full-repetition test as “Day One” test. The other two test were performed using the “frames” acquired on September the 13th while performing the first of the full-repetition tests.

INTER-OPERATOR TESTS [1 of 3]

		Section												N
		1	2	3	4	5	6	7	8	9	10	11	12	
Operator	1	X										X	X	
	2	X											X	
	3	X											X	
	4												X	

Specimen: 779
Vertebra: T4
Section: Inf

		Section												N
		1	2	3	4	5	6	7	8	9	10	11	12	
Operator	1	X	X								X	X	X	
	2	X								X	X	X		
	3	X	X	X					X	X	X	X		
	4										X	X		

Specimen: 779
Vertebra: T4
Section: Cen

		Section												N
		1	2	3	4	5	6	7	8	9	10	11	12	
Operator	1	X	X	X								X	X	
	2	X											X	
	3	X	X	X					X	X	X	X		
	4	X											X	

Specimen: 779
Vertebra: T4
Section: Sup

INTER-OPERATOR TESTS [2 of 3]

		Section												N
		1	2	3	4	5	6	7	8	9	10	11	12	
Operator	1												X	
	2	X	X									X	X	
	3												X	
	4												X	

Specimen: 779
Vertebra: T5
Section: Inf

		Section												N
		1	2	3	4	5	6	7	8	9	10	11	12	
Operator	1													
	2	X	X	X						X	X			
	3													
	4									X	X			

Specimen: 779
Vertebra: T5
Section: Cen

		Section												N
		1	2	3	4	5	6	7	8	9	10	11	12	
Operator	1													
	2													
	3													
	4													

Specimen: 779
Vertebra: T5
Section: Sup

INTER-OPERATOR TESTS [3 of 3]

		Section													
		1	2	3	4	5	6	7	8	9	10	11	12	N	
Operator	1														
	2								X						
	3														
	4														

Specimen: 779
Vertebra: T8
Section: Inf

		Section													
		1	2	3	4	5	6	7	8	9	10	11	12	N	
Operator	1		X	X	X								X		
	2		X	X	X										
	3		X		X					X			X		
	4		X		X										

Specimen: 779
Vertebra: T8
Section: Cen

		Section													
		1	2	3	4	5	6	7	8	9	10	11	12	N	
Operator	1			X	X	X	X								
	2			X	X	X									
	3			X	X	X	X							X	
	4			X	X	X									

Specimen: 779
Vertebra: T8
Section: Sup

NOTE: Inter-operator tests took place between October the 15th and October the 16th. The nine “frames” I used for the tests were obtained on the first day of the full-repetition tests. I tasked the operators with “locating the lytic metastases within the masks”. To avoid any *bias*, the tests were led separately.

Thanks are due to my four colleagues, who kindly volunteered to perform this test. Thanks to Anisha, Lorenzo, Marcella, and Matilde for the valuable help.

Additional Specimen

An additional specimen was provided by the department of pathological anatomy and histology of the Rizzoli Orthopedic Institute.

I chose to include its' analysis in this addendum, rather than the main body of the thesis, for two reasons: firstly, the testing of this specimen was conducted prior to the definition of a rigorous protocol; secondly, many information about the donors were not available.

The additional specimen (no. 753) was initially composed by the five lumbar vertebrae (i.e. from L1 to L5). Two metastatically involved vertebrae (L3 and L4, with L4 being the most relevant to study) were identified by the oncologist within the specimen. L4 and L3 were involved with blastic metastases.

A segment of two complete vertebrae was obtained from the original specimen. The segment included the vertebrae from L2 ½ to L5 ½.

After 20 cycles of preconditioning, the segment was tested in compression (wave form: monotonic ramp, 1 mm and 1.5 mm, 0.1m/s). Strains were acquired *via* DIC.

Peaks in the strain field ([figure A1](#) and [A2](#)) could be observed. However, these peaks were found on the surface of vertebra L3 (which was also metastatically involved).

When observing eps1, the strain field on L3 was like the one observed on the intervertebral disc. When eps2 were considered, the strain field showed both positive and negative, again in a pattern not dissimilar to that of soft tissues.

Given the distribution of the metastasis (the blastic lesion in vertebra L3 was not scattered homogeneously, as one could argue by observing [figure A3](#)), the “discontinuity” in the bony tissue might have caused a redistribution of the strains. But, can we rightly consider an osteoblastic lesion as a discontinuity in the bony tissue? The answer to the question would be far from trivial. In fact, the metastatic tissue is produced by the osteoblast, thus we could hypothesize that its formation should maintain a certain degree of homogeneity with the natural trabecular pattern.

However, the chance of having unremoved soft tissue to spoil the strain field should not be neglected.

Specimen 753 - Segment L2½-L5½

Engineering Principal Strain 1		
Vertebra	L3	L4
Mean (\pm SD)	150 (\pm 120)	560 (\pm 150)
Minimum	-348	-604
Maximum	2873	23700

Engineering Principal Strain 2		
Vertebra	L3	L4
Mean (\pm SD)	-170 (\pm 150)	-400 (\pm 160)
Minimum	-1040	-18614
Maximum	416	3394

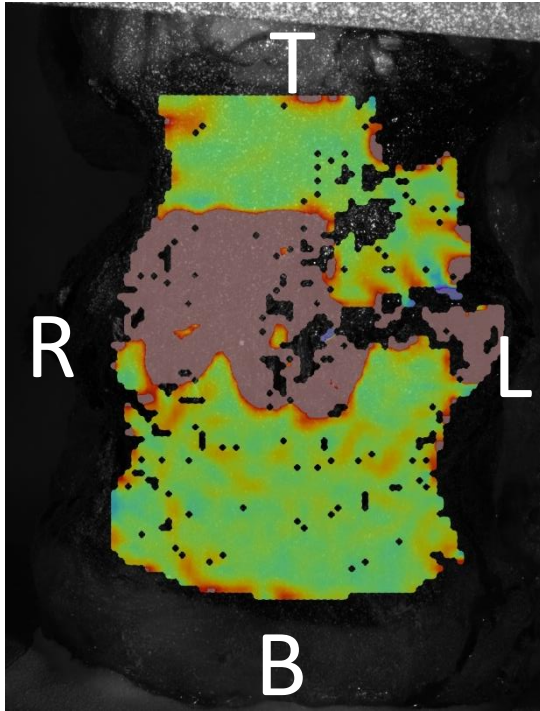


Figure A2 – Maximum eps (ϵ_1) for the segment L2½ - L5½. A significant peak can be observed on the surface of L3, in the lower corner of the right side.

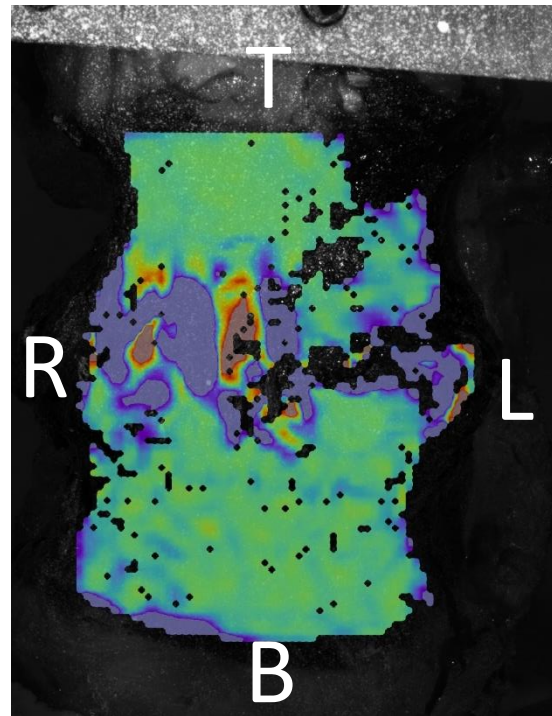


Figure A3 – Minimum eps (ϵ_2) for the segment L2½ - L5½. Both positive and negative peaks can be observed on the surface of L3, in the lower corner of the right side.

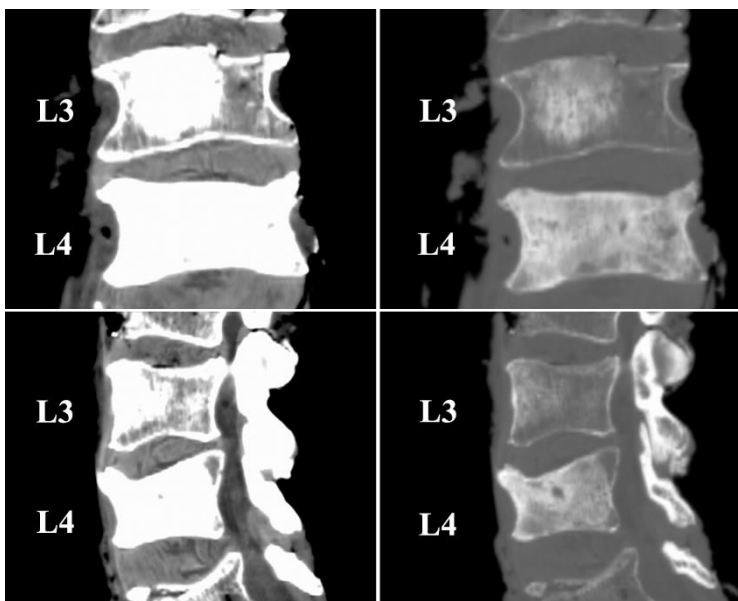


Figure A4 – Various view of vertebrae L3 and L4 from the CT-scans. Proceeding clockwise from the picture on the left upper corner:

- Frontal view (window mode: initial value);
- Frontal view (window mode: bone);
- Lateral view (window mode: bone);
- Lateral view (window mode: initial value).

References

- Alkalay, R. (2015). Effect of the Metastatic Defect on the Structural Response and Failure Process of Human Vertebra: An Experimental Study. *Clinical Biomechanics*, 121-128.
- Alkalay, R., & Harrigan, T. (2016). Mechanical Assessment of the Effects of Metastatic Lytic Defect on the Structural Response of Human Thoracolumbar Spine. *Journal of Orthopaedic Research*, 1808-1819.
- Anonymous. (2019, August 1). *Informati sul cancro: Glossario*. Retrieved from AIRC: <https://www.airc.it/glossario-tumori>
- Anonymous. (2019, August 7). *Patient Care: Services Offered: Quantitative Compute Tomography (QCT)*. Retrieved from University of California, San Francisco: Department of Radiology & Biomedical Imaging: <https://radiology.ucsf.edu/patient-care/services/QCT>
- Batson, O. (1940). The Function of the Vertebral Veins and Their Rôle in the Spread of Metastases. *Annals of Surgery*, 138-149.
- Brandolini, N., Cristofolini, L., & Viceconti, M. (2013). Experimental Methods for the Biomechanical Investigation of the Human Spine: A Review. *Journal of Mechanics in Medicine and Biology*, 1430002(1)-1430002(33).
- Bray, F., Ferlay, J., Soerjomataram, I., Siegel, R., Torre, L., & Jemal, A. (2018). Global Cancer Statistics 2018: GLOBOCAN Estimates of Incidence and Mortality Worldwide for 36 Cancers in 185 Countries. *CA: A Cancer Journal for Clinicians*, 394-424.
- Bunting, R. W., & Shea, B. (2001). Bone Metastasis and Rehabilitation. *Cancer Rehabilitation in the New Millennium*, 1020-1028.
- Charité – Universitätsmedizin Berlin. (2019, August 15). *OrthoLoad: Database*. Retrieved from OrthoLoad: <https://orthoload.com/database/>
- Chung, C. T., & Carlson, R. W. (2003). Goals and Objectives in the Management of Metastatic Breast Cancer. *The Oncologist*, 514-520.
- Coleman, R., & Rubens, R. (1987). The Clinical Course of Bone Metastases from Breast Cancer. *British Journal of Cancer*, 61-66.
- Costa, M., Eltes, P., Lazary, A., Varga, P., Viceconti, M., & Dall'Ara, E. (2019). Biomechanical assessment of vertebrae with lytic metastases with subject-specific finite element models. *Journal of the Mechanical Behavior of Biomedical Materials*, 268-290.
- Cristofolini, L. (2015). In vitro evidence of the structural optimization of the human skeletal bones. *Journal of Biomechanics*, 787-796.
- Cristofolini, L. (2015). Overview of Digital Image Correlation. In A. Freddi, G. Olmi, & L. Cristofolini, *Experimental Stress Analysis for Material and Structures* (pp. 187-213). Cham (Switzerland): Springer.
- Danesi, V., Zani, L., Scheele, A., Berra, F., & Cristofolini, L. (2013). Reproducible Reference Frame for In Vitro Testing of the Human Vertebrae. *Journal of Biomechanics*, 313-318.

- Ewing, J. (1922). *Neoplastic Diseases; a Treatise on Tumors*. London: Philadelphia London, W. B. Saunders company.
- Fidler, I. (2002). The Organ Microenvironment and Cancer Metastasis. *Differentiation*, 498-505.
- Fisher, C., DiPaola, C., Ryken, T., Bilsky, M., Shaffrey, C., Berven, S., . . . Fourney, D. (2010). A Novel Classification System for Spinal Instability in Neoplastic Disease. *Spine*, E1221-E1229.
- Griesmann, H., & Schüttemeyer, W. (1947). Weitere Erfahrungen mit der Marknagelung nach Kuntscher an der Chirurgische Universitätsklinik Kiel. *Der Chirurg*.
- Gupta, G. P., & Massagué, J. (2006). Cancer Metastasis: Building a Framework. *Cell*, 679-695.
- Hart, R. A., Boriani, S., Biagini, R., Currier, B., & Weinstein, J. N. (1997). A System for Surgical Staging and Management of Spine Tumors: A Clinical Outcome Study of Giant Cell Tumors of the Spine. *Spine*, 1773-1782.
- Mundy, G. (1997). Mechanisms of Bone Metastasis. *Cancer*, 1546-1556.
- Mundy, G. (2002). Metastasis to Bone: Causes, Consequences and Therapeutic Opportunities. *Nature*, 584-593.
- Orr, F. W., Kostenuik, P., Sanchez-Sweatman, O. H., & Singh, G. (1993). Mechanisms Involved in the Metastasis of Cancer to Bone. *Breast Cancer Research and Treatment*, 151-163.
- Paget, S. (1889). The Distribution of Secondary Growths in Cancer of the Breast. *The Lancet*, 571-573.
- Palanca, M., Barbanti-Bròdano, G., & Cristofolini, L. (2018). The Size of Simulated Lytic Metastases Affects the Strain Distribution on the Anterior Surface of the Vertebra. *Journal of Biomechanical Engineering*, 111005 (1) - 111005 (9).
- Palanca, M., Brugo, T. M., & Cristofolini, L. (2015). Use of Digital Image Correlation to Investigate the Biomechanics of the Vertebra. *Journal of Mechanics in Medicine and Biology*, 1540004(1)-1540004(10).
- Palanca, M., Marco, M., Ruspi, M. L., & Cristofolini, L. (2018). Full-field Strain Distribution in Multi-vertebra Spine Segments: An In Vitro Application of Digital Image Correlation. *Medical Engineering and Physics*, 76-83.
- Ratner, B., Hoffman, A. S., Schoen, F. J., & Lemons, J. E. (2013). *Biomaterials Science: An Introduction to Materials in Medicine*. Cambridge, MA: Academic Press.
- Roodman, G. (2004). Mechanisms of Bone Metastasis. *The New England Journal of Medicine*, 1655-1664.
- Silva, M., Hipp, J., McGowan, D., Takeuchi, T., & Hayes, W. (1993). Strength Reductions of Thoracic Vertebrae in the Presence of Transcortical Osseous Defects: Effects of Defect Location, Pedicle Disruption, and Defect Size. *European Spine Journal*, 118-125.
- Tantivejkul, K., Kalikin, L. M., & Pienta, K. J. (2004). Dynamic Process of Prostate Cancer Metastasis to Bone. *Journal of Cellular Biochemistry*, 706-717.

- Tschirhart, C., Nagpurkar, A., & Whyne, C. (2004). Effects of Tumor Location, Shape and Surface Serration on Burst Fracture Risk in the Metastatic Spine. *Journal of Biomechanics*, 653-660.
- Warburg, O. (1956). On the Origin of Cancer Cells. *Science*, 309-314.
- Whyne, C., Hu, S., & Lotz, J. (2001). Parametric Finite Element Analysis of Vertebral Bodies Affected by Tumors. *Journal of Biomechanics*, 1317-1324.
- Whyne, C., Hu, S., & Lotz, J. (2003). Burst Fracture in the Metastatically Involved Spine. *Spine*, 652-660.
- Windhagen, H., Hipp, J., Silva, M., Lipson, S., & Hayes, W. (1997). Predicting Failure of Thoracic Vertebrae With Simulated and Actual Metastatic Defects. *Clinical Orthopaedics and Related Research*, 313-319.
- Wolff, J. (1892). *Das Gesetz der Transformation der Knochen*. Berlin: Verlag August Hirschwald.

The end of a significant (and most intense) part of my journey is approaching.

Three years ago, when I enrolled at the University of Bologna, I was clueless about what was waiting for me.

As you might or might not know, three years ago I yearned for a rather different path.

Biomedical engineering was a diversion from that path.

Sometimes, I turn my mind to those years. I do not what kept me on this track for the first two years. For, you know, I do not have a knack for electronics, and those years, so focused toward forming electrical engineers, weighted heavy on my spirit.

While sometimes I regret those choices, I would do it all over again. Because those years of struggles brought me here. This path allowed me to discover biomechanics.

With that said, I thank the professor Luca Cristofolini, whose lecture were a source of inspiration, to which I grasped in a time where I was uncertain of the direction of my studies. His course allowed me to discover the wonders of mechanics, setting my path for my future studies.

While not being involved directly in this work, I want to thank Ph. D. Federico Morosato, who kindly assisted me during my internship. Being himself a biomedical engineer in a biomechanics laboratory, he has been a sort of example for me.

Lastly, the very father of this work, Ph. D. Marco Palanca.

I'm doubly in debt with Marco: once as professor and once as researcher.

Thanks to (professor) Marco Palanca, I'll never forgot what you taught me. When someone will ask me "What does stainless steel contains?", I'll always answer "Chromium or molybdenum, as well as **nickel**".

Thanks to (researcher) Marco Palanca, for supporting this work. Thank you for this and for passing onto us your enthusiasm.

Before I close. I want to address my sincerest thanks to you, the reader.

Thank you for taking your time to read this first (flawed) work.

Michele Serra